Endocranial Cast Anatomy of the Extinct Hipposiderid Bats Palaeophyllophora and Hipposideros (Pseudorhinolophus) (Mammalia: Chiroptera)

Jacob Maugoust, Maeva Orliac

!!! Manuscript before Proof's approval !!!!!

Endocranial cast anatomy of the extinct hipposiderid bats *Palaeophyllophora* and *Hipposideros* (*Pseudorhinolophus*) (Mammalia: Chiroptera)

Jacob Maugoust[1], Maeva J. Orliac[1]
Affiliation : [1]: Institut des Sciences de l'Evolution de Montpellier, UMR 5554 Université de Montpellier, CNRS, IRD, EPHE, place Eugène Bataillon, 34095 Montpellier cedex 5, France
Corresponding author: Jacob Maugoust (jacob.maugoust@umontpellier.fr, ORCID ID: 0000-0002-5525-7861)

Abstract

Bat fossil endocasts have been little studied in the literature (nine published works, only one in the XXIth century), and macromorphology of the brain of extant bats has only been characterized at the family-level. We describe here in detail the endocranial casts of four fossil hipposiderid species based on µCT-scans data and propose a revised nomenclature of the hipposiderid brain structures that leave their imprint on endocranial casts. Exhaustive comparisons of the external morphology of our fossil cranial endocast sample allow us to discuss the distribution of both qualitative and quantitative features in this family for different epochs. A conservatism of the brain is considered to be the rule during bats evolution. Indeed, we found that encephalization did not increase since the Eocene in hipposiderid bats (contrary to other mammals) and that macromorphology of the brain is close between Paleogene, Miocene, and extant hipposiderid species. However, subtler but promising fine anatomical characters might allow distinguishing genera and species. Eventually, expanding the fossil sample and/or adding extant species could shake the paradigm of temporal homogeneity and bring new light on the morpho-anatomical evolutionary history of Hipposideridae.

Keywords: endocast – Hipposideridae – Paleogene – brain – µCT-scan

Declarations

Funding: This work was, in part, financially supported by the ANR program DEADENDER (ANR-18-CE02-0003-01) headed by M. J. Orliac.
Competing interests: The authors declare having no competing interests.

Acknowledgements

We thank L. Costeur (NMBS) for access to the collections. We are grateful to the MRI platform member of the national infrastructure France-BioImaging supported by the French National Research Agency (ANR-10-INBS-04, «Investments for the future»), the labex CEMEB (ANR-10-LABX-0004) and NUMEV (ANR-10-LABX-0020). We also acknowledge Nicolas Brualla for the segmentation of the *Pa. quercyi* endocast and Romain Weppe for fruitful comments on the figures. This work was, in part, financially supported by the ANR program DEADENDER (ANR-18-CE02-0003-01) headed by M. J. Orliac. This is ISEM publication 2020-XX.

Introduction

In the middle of the last century, Tilly Edinger stated that paleoneurology could be regarded as the "little-known child of paleontology and neurobiology" (Edinger 1949:1). Indeed, study of internal structures of fossils, a fortiori endocranial cast, was then limited by the destructive nature of internal investigation of fossil skulls. Generalization of non-invasive techniques (especially µCT-scanning) now allows for enhanced access to endocranial structures and has led to an increased knowledge of mammal fossil endocasts. These techniques increasingly allow for discussing the evolutionary history of the brain, which may reflect both phylogenetic history and ecological constraints, through the external morphology of cranial cavity casts. Among mammals, bats are a remarkable group by their crucial contribution to extant mammal diversity (second most diverse order, e.g., Teeling 2009) and by their unique ecological specializations towards sustained flight combined with the ability to echolocate (e.g., Teeling et al. 2000). The specificity of their ecology is reflected by their brain anatomy, which has been documented for several extant species (e.g., Larsell and Dow 1935; Eisenberg and Wilson 1978; Jolicoeur et al. 1984; Baron et al. 1996; Safi et al. 2005; Bhatnagar et al. 2016). However, surprisingly, the evolutionary history of the brain characteristics of Chiroptera has barely been discussed. Our knowledge of the brain morphology of extinct bats so far relies on a small number of short descriptions performed in the second half of the XXth century on natural endocranial casts belonging to the families Hipposideridae, Emballonuridae, and Vespertilionidae (Edinger 1926, 1929, 1961, 1964a, b; Dechaseaux 1956, 1962, 1970, 1973). These works briefly compare the fossil endocasts with one another and with some extant representatives of the order. They show that, just like extant representatives, fossil bats had a low complexity of the telencephalon with a moderately expanded neopallium bearing no or few sulci and an exposed mesencephalon.

These traits are described as “primitive” features that would have been maintained through time (Edinger 1964a, b). More recently, Yao et al. (2012) included fossil data in their study on the evolution of the relative brain size in Hipposideridae, but provided no morphological description. To date, there is no formal description of a fossil bat endocast, no formal thorough/extensive comparison between extant and fossil species, and no integrative (i.e., qualitative and quantitative) discussion of the evolutionary history of the bat brain.

Regarding Chiroptera diversity, according to Amador et al. (2018), there are today 21 families and more than 1200 recognized species split into two suborders (ESM1: Fig. SI. 1), Yangochiroptera (with three superfamilies of echolocating “microbats”: Emballonuroidea, Noctilionoidea, and Vespertilionoidea), and Yinpterochiroptera (gathering the echolocating “microbat” superfamily Rhinolophoidea and the non-echolocating “megabat” family Pteropodidae). The phylogenetic relationships supporting this rather recent systematic framework of Chiroptera raise questions about the evolutionary history of the whole group, especially regarding the acquisition of flight and of sophisticated echolocation of the paraphyletic “microbats” (e.g., Teeling et al. 2002). The fossil record of the order remains however fragmentary (Eiting and Gunnell 2009); Brown et al. (2019) identified 167 fossil genera and 441 fossil species, adding eight additional extinct families to the extant ones. They also highlighted the pretty low osteological preservation for bats, related to their very light skeleton adapted to flight. Regarding the brittleness of their cranium, a three-dimensional preservation of the braincase is therefore quite exceptional in the fossil record. Yet, a few fossil bats crania and natural endocasts provide an opportunity to investigate in detail the endocranial structures of chiropterans using micro-CT scanner imaging techniques. Cave deposits are most favorable for the preservation of bat skeletons (Brown et al. 2019); Quercy Phosphorites (SW France) are karstic infillings that yielded a tremendous amount of fossil bat material (17.6% of the world fossil bat record according to Brown et al. 2019), with a high taxonomic diversity (six families including three extinct, 11 genera and 46 species according to Brown et al. 2019), and ranging from the middle Eocene to the early Miocene (Maitre 2014). The few endocasts described by Dechaseaux (1956, 1962, 1970, 1973) and Edinger (1926, 1929, 1961, 1964a, b) mainly come from this geological formation where numerous natural endocasts and skulls have been collected (e.g., Maitre 2014).

Among extant bat families, Hipposideridae occupy the second rank in terms of specific diversity in the whole fossil record of the order (Brown et al. 2019) and the richest in the Quercy Phosphorites fossil record (Maitre 2014). These bats are commonly known as the “Old World leaf-nosed bats” and belong to the superfamily Rhinolophoidea. They appear in the fossil record in the middle Eocene of Europe (Maitre 2014; Brown et al. 2019) and nowadays include ten living genera and around 80 species, 70 of which are comprised in the widespread genus *Hipposideros* (Simmons 2005; Foley et al. 2017). This family is the sixth most diverse bat family (Shi and Rabosky 2015; Amador et al. 2018), just after the Rhinolophidae. They represent together the major part of the rhinolophoid superfamily (81 hipposiderid and 83 rhinolophid species of the 183 rhinolophoid species according to Amador et al. (2018)). The brain of modern Hipposideridae has been briefly described in the literature (Baron et al. 1996) and endocasts of extinct Hipposideridae are so far known through very succinct descriptions only (Edinger 1926; Dechaseaux 1956, 1962). However, cranial remains of fossil Hipposideridae are often well preserved (and particularly braincases; Brown et al. 2019). This makes this family a good candidate to investigate their brain evolution through endocasts and to set the basis for future studies on bat endocranial casts.

We propose here the first nomenclature of the external morphological features of the bat's brain, and we describe and compare in detail endocranial casts of extinct hipposiderid bats based on four species (Fig. 1): *Palaeophyllophora oltina*, *Palaeophyllophora quercyi*, *Hipposideros* (*Pseudorhinolophus*) *bouzigensis*, and *Hipposideros* (*Pseudorhinolophus*) *schlosseri*. We discuss general and detailed brain macromorphology of hipposiderid bats, together with common measurements of endocasts (EQ, olfactory bulb volume, paraflocculi volume). We finally propose the first hypotheses on the evolutionary history of the hipposiderid brain.

Material and methods

Taxa and specimens

We investigate and describe the external features of the brain through the reconstruction of the cranial endocasts of four fossil species belonging to two genera of the family Hipposideridae. Each species is represented by a single specimen housed in the University of Montpellier (UM, France) or in the Naturhistoriches Museum Basel (NMBS, Switzerland):

- *Palaeophyllophora oltina* is documented by a partial cranium with braincase almost complete (NMBS QP784), which comes from the locality of Sainte-Néboule (Quercy, Lot, SW France) of Mammalian Paleogene standard level 18 ("MP18"; i.e., biostratigraphic assemblage zones in the stratigraphic record of the Paleogene period of Europe; Schmidt-Kittler 1987) age (upper Eocene; Maitre 2014);

- *Palaeophyllophora quercyi* is documented by a partial cranium with braincase almost complete (UM ACQ 6627), which comes from ancient Quercy collections of indeterminate age and precise provenance (except Quercy area, SW France);

- *Hipposideros (Pseudorhinolophus) schlosseri* is documented by a natural cranial cast (NMBS QV 370) from ancient Quercy collections, also with indeterminate age and precise provenance;

- *Hipposideros (Pseudorhinolophus) bouziguensis* is documented by a natural cranial cast (NMBS G 2369) from the locality of Bouzigues (S France) of Mammalian Neogene unit 2a ("MN2a"; Mein 1975) age (lower Miocene; Sigé 1968).

We compared these four fossil species to the extant *Hipposideros diadema*, whose figures (Baron et al. 1996: figs. 8, 24 and 40) are, to our knowledge, the only illustrations in the literature (for bats) with a sufficient quality to investigate brain external morphology. Specimens of *H. (Ps.) schlosseri* and *H. (Ps.) bouziguensis* have been figured in Yao et al. (2012) but not described. We quickly mention them in the description of the corresponding taxa.

Taxonomic framework

A huge work of systematic paleontology has been done by Maitre (2014) who greatly clarified taxonomy of extinct bat species from Quercy deposits; we follow her work for the attribution of our three Quercy specimens (that are *Pa. oltina*, *Pa. quercyi* and *H. (Ps.) schlosseri*), which were already attributed to valid species names. Regarding *H. (Ps.) bouziguensis*, no work has been done since the works of Sigé (1968), Legendre (1982), and Sigé et al. (1997); we thus trust the former attribution of our Bouzigues specimen.

Within Hipposideridae, relationships of extant species are getting resolved (Foley et al. 2015, 2017), but phylogenetic relationships of extinct species are poorly studied and diverge depending on the analyses (see Hand and Kirsch 2003; Ravel et al. 2016; Wilson et al. 2016). We rather follow the results of Ravel et al. (2016) because they aim to decipher relationships between extinct species rather than placing them within a constrained extant species framework; besides, their matrix included both craniodental and postcranial characters. A pruned topology of Ravel et al. (2016) including the species of our sample is presented in Fig. 1.

Data acquisition

Three dimensional data acquisitions of the four specimens were performed using the µ-CT facilities in the University of Montpellier (MRI; ISEM): *Pa. quercyi* was scanned using a Skyscan 1076 µ-CT and the three other species were scanned using a EasyTom 150 µ-CT. The voxel resolution is 18.08µm for *Pa. quercyi*, 23.82µm for *Pa. oltina*, 35.72µm for *H. (Ps.) schlosseri* and 23.81µm for *H. (Ps.) bouziguensis*. Other details regarding the acquisition parameters are summarized in ESM2: Table SI. 1. Segmentation and volumetric measurements of each specimen were performed using Avizo ® 9.3 (Thermo Fisher Scientific-FEI) and visualization was done using MorphoDig © (Lebrun 2018). Figures illustrating the cranial endocasts were done using Inkscape © (Inkscape Project 2018, v0.92.3) and other figures were done using Photofiltre © (Da Cruz 2015, v7.2.1). Linear measures were taken on the outline of each structure using both Inkscape and Photofiltre. Sagittal angles were taken using MorphoDig and ImageJ (Schneider et al. 2012, v1.48).

Encephalization

Encephalization quotient of a species (EQ; Jerison 1973) is the ratio between the observed mass of the brain of this species (E) over the expected mass of the brain of this species (E_e) given its body mass (M). The value of the ratio gives then an idea of the "encephalization" of the species: if the ratio is over one, the brain is "larger" than expected, and vice versa. The tricky point concerns the calculation of the expected mass of the brain. The original formula of Jerison (1973) is $\mathrm{EQ}_{\mathrm{Jerison}} = \frac{\mathrm{E}}{0.12 \times \mathrm{M}^{\frac{2}{3}}}$. However, Eisenberg and Wilson (1978) noted that Jerison (1973) defined this formula based on a mammalian-scale sample underrepresenting bats. They proposed another formula, including more mammals and especially more bat species: $\mathrm{EQ}_{\mathrm{Eisenberg}} = \frac{\mathrm{E}}{0.055 \times \mathrm{M}^{0.74}}$. We calculated EQ for our four fossil bat species using these two formulas, but mainly discussed EQ based on the equation of Eisenberg and Wilson (1978).

In order to compare EQ values of various mammal species through time, we gathered body and brain masses of several fossil and extant mammal species from the literature (Silcox et al. 2010; Shultz and Dunbar 2010; Orliac and Gilissen 2012; Ramdarshan and Orliac 2016; Bertrand et al. 2018a, b). Bats are absent from these datasets, so we added the extant bat data from Baron et al. (1996) and Bhatnagar et al. (2016) (ESM2: Table SI. 2). For *H. (Ps.) schlosseri*, we used the brain mass value provided by Yao et al. (2012) because of the partial preservation of the specimen described here. Moreover, the temporal extension of the latter species covers both the Eocene and Oligocene epochs; as we do not know it precise age, we duplicated this value with an Eocene and an Oligocene age for each duplicate.

Maitre (2014) provided body mass estimates for each chiropteran species from Quercy, in each MP, based on the area of the first lower molar. We used the body mass estimate value of Maitre (2014)

for *Pa. oltina* as this species is found only in the MP18 site of Ste-Néboule, from which the endocast described here derives. We considered the mean value of the different body masses through time for *Pa. quercyi* and for *H. (Ps.) schlosseri* because the precise provenance – and therefore precise age – of these specimens is unknown. We calculated the body mass of *H. (Ps.) bouziguensis* by taking the mean values of length and width of the first lower molars provided by Sigé (1968) and using the equation of Maitre (2014).

Statistical treatment of the EQ data was done using R (R Core Team 2018, v3.5.0) and its interface RStudio (RStudio Team 2016, v1.1.453) using package FSA (Ogle et al. 2019) in addition to built-in packages. EQ values for mammals are visually compared through Cenozoic epochs by plotting boxplots. We use a Shapiro-Wilk test (Shapiro and Wilk 1965; Royston 1995; `shapiro.test` function) of normality to know (at a 5% risk) if the various samples used are normally distributed. To know (at a 5% risk) if there is an homogeneity or not in the EQ values of a group through Cenozoic epochs, we use either a Kruskal-Wallis test (Kruskal and Wallis 1952; Hollander and Wolfe 1973; `kruskal.test`), also known as a "non-parametric ANOVA," if the sample was not normally distributed, or both a Kruskal-Wallis test and a Fisher test (Fisher 1970; Chambers and Hastie 1991; `anova` and `lm` functions) if the sample was normally distributed; in most cases, samples were not normally distributed so we kept Kruskal-Wallis even if it was the case. When there was a difference (i.e., a significant p-value), we used either non parametric Dunn's pairwise tests (Dunn 1964; `dunnTest` function of FSA package) or both parametric Tukey HSD (Tukey 1949; `TukeyHSD` function) tests and non-parametric Dunn's pairwise tests to know (at a 5% risk) which pair(s) were different.

As an additional graphical representation of the EQ formulas, we plotted the log brain masses against the log body masses (using natural logarithms) and we added to the plot the regression lines derived from the EQ formulas of Eisenberg and Wilson (1978) and Jerison (1973). Indeed, the expected brain mass for a given body mass is a $a.X^b$ relationship; the expected log brain mass for a given log body mass is thus $b.\log(X)+\log(a)$. Eisenberg and Wilson (1978) proposed an expected brain mass formula which is $0.055 \times M^{0.74}$; the expected log brain mass is thus $0.74 \times \log(M) + \log(0.055)$; the regression line used here is therefore $y = 0.74 \times \log(x) + \log(0.055)$. In a similar way, regarding the expected brain mass formula of Jerison (1973), the regression line is $y = 2/3 \times \log(x) + \log(0.12)$.

The use of EQ values to compare encephalization between extinct taxa has received some criticism, notably regarding the uncertainty related to body mass estimates (e.g., Smith 2002; Alba 2010; Millien and Bovy 2010; Gingerich 2016; Ramdarshan and Orliac 2016). Moreover, brain masses are estimated based on partially preserved material for two of our four fossil species. We therefore remain cautious concerning the use of EQ values to qualify/quantify brain evolution through time.

Other endocast measurements

A common measurement on endocasts is the telencephalic flexure, or "cranial base angle" (Ramdarshan and Orliac 2016). However, the term "telencephalic" flexure is used to describe a bending of the telencephalon (and only it) that occurs during ontogeny. This angle between the ventral planes of the telencephalon and rhombencephalon in general rather corresponds to the definition of the cephalic flexure (Nieuwenhuys 1998). Another flexure that can be measured on endocasts is the cervical flexure (Nieuwenhuys 1998), a bending between the rhombencephalon and the spinal cord. This flexure can be measured by adding 90° (considering the major axis of the foramen magnum perpendicular to the orientation of its opening) to the angle between the ventral plane of

rhombencephalon and the great axis of the foramen magnum (a line whose extremities are the most dorsal and the most ventral points of the foramen magnum in lateral view).

We also calculated volumes of "individualizable parts" of the brain, which are that of the olfactory bulbs (e.g., Jerison 1973; Orliac and Gilissen 2012; Benoit et al. 2013; Ramdarshan and Orliac 2016) and of the paraflocculi (e.g., Bertrand et al. 2018a, b, 2019). The volumes of these structures are inferred from the volumes of their containing cavities. The real volume of the olfactory bulbs and paraflocculi may differ from our measurement (e.g., if bulbs are partly covered by the cerebrum or if the subarcuate fossa encloses additional structures to the paraflocculi). One should therefore remain cautious regarding interpretations on these measures. Regarding olfactory bulbs volume, we used the datasets of Baron et al. (1996) and of Bhatnagar et al. (2016), which include more than 270 extant species, and we added values for our fossil species (ESM2: Table SI. 3). Regarding parafloccular volume, no substantial dataset is available for bats in the literature; we therefore compared our fossil sample to the small sample of mammals – including some bat species – provided by Ferreira-Cardoso et al. (2017) to which we added the values of some extant and extinct rodents from Bertrand et al. (2018a, b) (ESM2: Table SI. 4).

As these measurements likely are affected by allometry, we plotted log-volumes (to avoid allometric bias) of each against that of the whole brain (using natural logarithms). Our goal is not to characterize evolution of olfactory bulb relative volume or parafloccular relative volume through bat lineages (for the former) or mammalian lineages (for the latter), but simply to visualize where fossil bats lie compared to extant ones. Thus, we do not apply any PCM (Phylogenetic Comparative Method), such as PIC (Phylogenetic Independent Contrasts; Felsenstein 1985) or PGLS (Phylogenetic General Least Squares; Grafen 1989) regressions.

Data availability

Fossil material is housed in the UM (University of Montpellier, Montpellier, France) and NMBS (Naturhistorisches Museum Basel, Basel, Switzerland). µCT-data and 3D surfaces are available upon reasonable request. Datasets (CT-data acquisition parameters, brain and body volumes, EQ's, olfactory bulb volumes, paraflocculi volumes and test results) are provided in ESM2 (Tables SI. 1-5). The R code written and used for analyses in this paper is available in ESM3; see ESM4-6 for the raw datasets used in the code.

Nomenclature and homologies of the chiropteran brain structures

To date, no detailed study of chiropteran endocasts has been performed. Therefore, prior to describing the endocranial casts of extinct bat species from Quercy deposits, we need to properly identify and name the different observed structures. Various terms have been used across descriptions of endocast in other mammalian order, and, most of the time, discrepancies exist between paleoneurological and/or neurobiological studies. Consequently, we assess primary homologies of the chiropteran endocast structures and we choose and list the anatomical terms to use in future bat cranial cast descriptions. Unless otherwise discussed, we use Anglicized terms derived from the terminology of the 6th edition of the Nomina Anatomica Veterinaria (NAV 2017) .

Major components of the chiropteran brain observed on endocasts (Fig. 2)

The vertebrate brain is composed of: i) the prosencephalon, anteriorly (the "forebrain"), which is divided in a **telencephalon** and a **diencephalon**, ii) the **mesencephalon,** medially (the "midbrain"),

and iii) the rhombencephalon, posteriorly (the "hindbrain"), which is divided in a **metencephalon** and a **myelencephalon** (e.g., Barone and Bortolami 2004).

The telencephalon represents a major part of the brain (Fig. 2) and is composed of the **paleopallium** ventrally (with the **olfactory bulbs** at the anterior extremity and the **piriform lobes** posteriorly) and of the **neopallium** dorsally (a specific feature of mammals; Rowe et al. 2011). The paleopallium and the neopallium are separated by the **rhinal fissure** (Smith 1902a; Dechaseaux 1962; see below). The olfactory bulbs protrude anteriorly and are separated from the cerebral hemispheres (or "cerebrum," which contains the other telencephalic structures) by the **circular fissure**.

Regarding the diencephalon, the only parts visible on endocasts (Fig. 2) are the **epiphysis** dorsally and the **hypophysis** ventrally, also called the pineal gland and pituitary gland, respectively, in the NAV. We use the terms epi-/hypophysis because of their common root, which reflects their common general origin.

As for the mesencephalon, only the tectum mesencephali (or "**tectum**") is exposed (Fig. 2a) and the main recognizable structures are the corpora quadrigemina, or colliculi. These colliculi are disposed in two pairs which are the **rostral** (also called "superior" or "anterior") and **caudal** (also called "inferior" or "posterior") **colliculi** (according to the NAV).

The metencephalon is, dorsally, only represented by the **cerebellum** (Fig. 2a). Following the NAV, the cerebellum is medio-laterally composed of a **vermis** (or median vermis) in a median position, two **cerebellar hemispheres** lateral to the vermis, and two **paraflocculi** varying in position relative to the hemispheres (from ventral to lateral). In bats, the flocculi are small compared to the paraflocculi, and overshadowed during cerebellar ontogeny (Larsell and Dow 1935); it is unlikely that they can be observed on bat endocasts. The exposed part of the vermis is antero-posteriorly subdivided in a maximum of five lobules: the **declive** (lobule VI), the **folium vermis** (lobule VII A), the **tuber vermis** (lobule VII B), the **pyramis** (lobule VIII), and the **uvula** (lobule IX) (Dow 1942; Horikawa and Suga 1986; NAV 2017). The lobule X, or nodula, of the vermis is here not considered as a potential exposed part of the vermis because, in all bats, the cerebellum is bent and the nodula is fully internal. The cerebellar hemispheres ontogenetically develop from the tuber vermis and the folium vermis (Larsell and Dow 1935), forming two (**anterior** and **posterior**) **crura**. The declive, anterior to the two latter lobules, is also exposed. Larsell and Dow (1935) did not recognize a contribution from the declive to the cerebellar hemispheres in the species they studied (*Corynorhinus* sp.). However, in the case of an anterior expansion of the cerebellum, i.e., with an elongated vermis and elongated hemispheres, the declive could expand laterally and contribute to the hemispheres together with the tuber and folium vermis (Dow 1942). This anteriormost lobe of the cerebellar hemisphere is here named the **crus 0**. In ventral view (Fig. 2b), another part of the metencephalon is visible: the **pons**, located between the cochleae, posterior to the hypophysis.

Immediately posterior to the pons, the myelencephalon is visible as the **medulla oblongata** (Fig. 2b). A potential difficulty when studying endocasts is to separate these two contiguous structures. In Chiroptera, as illustrated by Baron et al. (1996) through sagittal sections, depending on taxa, there is no or very subtle separation on the brain (when a separation is present, it is a slight groove). Moreover, their relative position varies among bats: they can be both exposed ventrally (as for *Pteropus lylei* or *Dobsonia praedatrix*, Baron et al. 1996: figs. 51-52), or the pons can be positioned dorsal to the hypophysis and therefore not exposed ventrally (as for *Rhinolophus hipposideros* or

Mormoops megalophylla, Baron et al. 1996: figs. 53-54). For these two reasons, on endocasts the region between the (cast of the) hypophysis and the foramen magnum will be called a "**pons-medulla oblongata continuum.**"

General remarks on the exposed "foldings" of the brain

The telencephalon and the metencephalon are more or less folded in mammals, depending on the orders. Depending on the authors, these foldings are either called "fissures" or "sulci." Here, we rather follow Smith (1902a) than the NAV in calling a "fissure" any groove that obviously separates a structure from another (such as the "rhinal fissure" of the telencephalon, separating the paleopallium and the neopallium, or the secondary fissure (fissura secunda) of the metencephalon, separating lobules VIII and IX throughout the cerebellum) and a "sulcus" any groove on the surface of a structure (such as, in an endocast description, any groove visible at the surface of the neopallium). For instance, the NAV refers to the rhinal fissure as the sulcus rhinalis and to the pseudosylvia and suprasylvia as the fissura pseudosylvia and the sulcus suprasylvius respectively; yet, the pseudosylvia and the suprasylvia are both foldings on the neopallium, while the rhinal fissure separates different entities of the telencephalon, the paleopallium and the neopallium. Here, we therefore use the terms pseudosylvian sulcus, suprasylvian sulcus, and rhinal fissure.

Neopallial foldings and lobes (Fig. 3)

We follow Smith (1902a) for the definition of the main sulcus on the neopallium (Fig. 3a): from the rhinal fissure originates the pseudosylvia (or pseudosylvian sulcus, 'Ps.s' in Fig. 3a), directed dorsally. The primary organization of mammalian brain foldings is a concentric organization of sulci around the pseudosylvia due to a flexion of the telencephalon (the telencephalic flexure per se), with the ectosylvian ('E.s' in Fig. 3a), the suprasylvian ('S.s' in Fig. 3a), and the lateral sulci ('L' in Fig. 3a; Smith 1902a: fig. 2; Dechaseaux 1962). The lateral sulcus is posteriorly followed by the postlateral sulcus ('Po.L' in Fig. 3a) and preceded anteriorly by the coronal sulcus ('Co' in Fig. 3a); the coronal and the lateral can merge to form a coronolateral sulcus (Dechaseaux 1962). The suprasylvia is posteriorly followed by the postsylvia ('Po.s' in Fig. 3a); the suprasylvia and the postsylvia can also merge together, but in most cases, there is a marked angle between the two so they can be distinguished. Dechaseaux (1962) also recognized a presylvia, directed anterodorsally and anterior to the pseudosylvia, extended even more anteriorly than the coronal sulcus. Smith (1902a) called this structure the orbital sulcus ('O' in Fig. 3a); this term is also used by Baron et al. (1996) in their review of the bat brain, and we therefore use it here too. Smith (1902a) also recognized a cruciate sulcus ('Cr' in Fig. 3a), which is located rather anteriorly (at the level of the coronal and orbital ones), medial to the lateral sulcus and rather in a transverse orientation (as for the postlateral and the orbital ones).

The ectosylvia can be divided into an anterior part (between the suprasylvia and the pseudosylvia; 'E.s ant' in Fig. 3a) and a posterior part (between the pseudosylvia and the postsylvia; 'E.s post' in Fig. 3a), which could merge (Dechaseaux 1962: fig. 12) or not (Friant 1932: fig. 1). However, the ectosylvia is rather a carnivoran feature (Smith 1902a); it is sometimes also referred to in other groups such as ruminants (Anthony 1934) or manatees (Friant 1954), but results from the operculization of the two first arcuate gyri (cf. below; see arrows Fig. 3b-3d and Fig. 3c-3e), rather than being a "true" ectosylvian sulcus (as defined in carnivorans by Smith 1902a). What is mentioned as an "ectosylvian sulcus" in non-carnivorans by Anthony (1934) and Friant (1954) is the operculization sulcus ('Op.su' in Fig. 3d-e), a long sulcus bent anteriorwards resulting from the operculization.

According to Smith (1902a), the only "true" sylvian sulcus is a fusion of the pseudosylvia and the suprasylvia, and is a "complex of two sulci" (see arrow Fig. 3c-3f). Dechaseaux (1962) shared the same global sulcal scheme but rather defined a "sylvian complex," which results from an operculization that covers (and then hides) the pseudosylvia. These two structures are thus distinct and can be distinguished as follows: i) the "sylvian sulcus" ('Sy.su' in Fig. 3f-g) of Smith (1902a) is a single sulcus anteriorly connected to the rhinal fissure and bent posteriorwards, and ii) the "sylvian complex" ('Sy.cplx' in Fig. 3d-e) of Dechaseaux (1962), mainly bent dorsally, joins the rhinal fissure ventrally through the operculization sulcus.

In addition to those sulci, Dechaseaux (1962) names primary convolutions (Fig. 3b): i) the arcuate gyrus 1 between the rhinal fissure and the ectosylvia (around the pseudosylvia), ii) the arcuate gyrus 2 between the ectosylvia and the suprasylvia, iii) the arcuate gyrus 3 between the suprasylvia and the lateral sulcus, and iv) the reuniens gyrus between the orbital sulcus and the anterior portions of the arcuate gyri 1 and 2. When there is a "sylvian complex" (Fig. 3d-e), the arcuate gyrus 1 is operculized (i.e., covered by the arcuate gyrus 2) and not visible (Dechaseaux 1962). When there is no operculization or ectosylvia (Fig. 3c), the arcuate gyri 1 and 2 are not separated by the ectosylvia and form therefore one arcuate gyrus 1-2, and the reuniens gyrus is located between the orbital sulcus and the anterior arm of this arcuate gyrus 1-2. When there is a "sylvian sulcus" (Fig. 3f), there is no gap anymore between the pseudosylvia and the suprasylvia, and no more between the suprasylvia and the rhinal fissure, but there is still a gap between the postsylvia (or posterior part of suprasylvia) and the rhinal fissure; only remains the posterior portion of the arcuate gyrus 1-2. The reuniens gyrus is therefore located between the orbital sulcus and the "sylvian sulcus." The chiropteran brain is considered to lack gyri strictu senso (their brain is lissencephalic; Baron et al. 1996) and the term "lobe" is preferred to name surfaces between sulci. Moreover, among the sulci defining the different lobes, the single recognizable one in our fossil sample is the sylvian sulcus, or sylvia (Fig. 3g). We therefore use the term of reuniens lobe for the surface anterior to the sylvia, the term arcuate lobe for the surface posterior to the sylvia if the suprasylvia is not extended posteriorly (if it is the case, no distinction could be made between the posterior arm of the arcuate gyrus 1-2 and the arcuate gyrus 3), or the terms ventral and medial arcuate lobes for the surfaces posterior to the sylvia and respectively ventral and medial to the posterior extension of the suprasylvia (the ventral arcuate lobe is close in its morphological definition to the posterior portion of the arcuate gyrus 1-2, as is the lateral arcuate lobe to the posterior portion of the arcuate gyrus 3).

Cerebellar foldings (Fig. 2)

The five dorsally exposed cerebellar lobules of the metencephalon are separated by a minimum of four grooves, likely to be present on the exposed vermis (Fig. 2a). The first two have not been named and they separate lobules of the vermis restrictively, so they are here recognized as the VI-VII sulcus (separating lobules VI and VII) and the VII sulcus (separating lobules VII A and VII B). Barone and Bortolami (2004) named the VI-VII sulcus the fissura preansiformis as it separates lobules VI and VII, both in the vermis and in the cerebellar hemispheres. However, such a continuity is not obvious in bat brains (Horikawa and Suga 1986), and as the epithet of the fissure rather characterizes the cerebellar hemispheres, it will not be used here for a sulcus on the vermis surface. Barone and Bortolami (2004) also described a continuity between the vermis and the hemispheres and separated the folium vermis and the anterior crus from the tuber vermis and the posterior crus by the fissura intercruralis. The continuity between the vermis and the hemispheres has not been highlighted in bats

(Larsell and Dow 1935) and in mammals in general (Dow 1942), so unless such a continuity is seen, the sulcus separating tuber and folium vermis of the vermis is called here the sulcus VII. Posteriorly is the prepyramidal fissure (fissura prepyramidalis in Barone and Bortolami 2004; Fig. 2a). This fissure is referred to as the sulcus prepyramidalis by Dow (1942), separating lobules VII and VIII, but it expands laterally (Horikawa and Suga 1986) and is in fact continuous with the fissura paraflocculari s (Larsell and Dow 1935; Dow 1942); we therefore recognize this structure as a "fissure" (as do Barone and Bortolami 2004). The posterior-most groove is the secondary fissure (fissura secunda, the only cerebellar groove recognized by Baron et al. 1996): it separates the lobules VIII and IX but it also expands laterally (to where lie, anteriorly, the cerebellar hemispheres; Fig. 2a) (Horikawa and Suga 1986) and even inside the paraflocculi (Smith 1902b; NAV 2017), formed from parts of the lobules VIII and IX (Larsell and Dow 1935; Dow 1942). There can be additional sulci within each lobules when cerebellum complexifies (as seen in Baron et al. 1996: figs. 51-56).

The anterior and posterior crura of the cerebellar hemispheres are separated by the intercrural sulcus (Larsell and Dow 1935; Dow 1942), which is not continuous with the VII sulcus (Fig. 2a). If there is a crus 0 of these hemispheres, an additional sulcus is expected, anterior to the intercrural sulcus, and is therefore named the anterocrural sulcus, because it separates the two crura (1-2) from the crus 0. It would be equivalent to the VI-VII sulcus, but not necessarily in its continuity, as for the intercrural sulcus and the VII sulcus.

Not much attention has been paid to the parafloccular morphology. Larsell and Dow (1935) recognized a lateral sulcus of the paraflocculus on its lateral aspect but it could simply correspond to the lateral expansion of the secondary fissure, which would be congruent with Smith (1902b). Nothing more is known about potential grooves on the surface of these structures. In hipposiderid bats described here, there is a ventral groove. Without any other reference, it will be called a ventral sulcus of the paraflocculus (Fig. 2b).

Casts of braincase openings

The mesencephalon, the pons (from metencephalon), and the medulla oblongata (from myelencephalon) together form a functional unit which is the brainstem (Barone and Bortolami 2004). From this structure, 12 "cranial nerves" exit. These nerves exit the braincase through foramina visible in ventral view for most of them (Fig. 2b). Other cranial foramina are pathways for other fundamental structures and also need to be identified. Skull foramina in Chiroptera have only been recognized for the genus *Pteropus* (Giannini et al. 2006). We rely on this work for most of the openings we describe in Hipposideridae. However, some of them deserve a bit more attention because they appear to vary among Chiroptera (at least, between pteropodids and hipposiderids). The first is the sphenorbital fissure, where at least exit the oculomotor (III), trochlear (IV), ophthalmic branch of trigeminal (V1), and abducens (VI) nerves, can be coalescent with the optic foramen and/or with the round foramen, therefore being also the exit of the optic (II) and maxillary branch of the trigeminal (V2) nerves. The second is the ethmoidal foramen, which in *Pteropus* is located in the frontal or between the frontal and the orbitosphenoid but which here, on endocasts, appears on the lateral aspect of the olfactory bulb cast.

The orbitotemporal canal

Finally, the orbitotemporal canal, which carries the anterior division of the superior ramus of the stapedial artery (Giannini et al. 2006; Orliac and O'Leary 2014) deserves special attention as it is

largely thought to be a hallmark of the rhinal fissure position (e.g., Silcox et al. 2010; Bertrand and Silcox 2016; Ramdarshan and Orliac 2016). However, it is not always the case across mammals; for instance, the orbitotemporal canal can be in a more ventral position (Pantodonta, *Alcidedorbignya*, Muizon et al. 2015; Artiodactyla, *Homacodon*, Orliac and Gilissen 2012). In specimens described here, the orbitotemporal canal is visible (Fig. 2a): there is a marked longitudinal cast that runs parallel to the anterolateral side, it then reaches the posterolateral side of the telencephalon. In lateral view, it has in its first half a highly dorsal position, then it dives ventrally until it ends to a medial position, anterior and lateral to the petrosal bone. In the literature, the tissues surrounding the brain are removed during the preparation of fresh brains (see Baron et al. 1996); therefore, blood structures like the superior ramus of the stapedial artery are not reported on illustrations. Giannini et al. (2006) identified the orbitotemporal canal in *Pteropus*: it is a not-fully enclosed sulcus on the inner surface of the parietal and squamosal bones. We can identify the cast of this sulcus on endocasts, even if it is located in a more dorsal position than the rhinal fissure. However, these two structures join anteriorly. So, even if this canal is not a landmark of the rhinal fissure as a whole, its anterior extremity seems to be a good marker of the anterior location of the rhinal fissure.

Descriptions and comparisons

Endocranial cast of *Palaeophyllophora oltina*

Overall shape

The cast of the braincase of *Pa. oltina* (Figs. 4-5, see also Fig. 6 and ESM1: Figs. SI. 2-6) was virtually reconstructed from a cranium of the Naturhistoriches Museum Basel collections (NMBS QP784). The endocranial cast largely fills the posterior part of the cranium (Fig. 4); the cranial bones around the cranial cavity are very thin. The endocranial cavity extends anterior to the postorbital constriction, where lie the olfactory bulbs.

It has a total volume of 525.9 mm^3 (Tables 1-2). In dorsal view (Fig. 5a-b), its shape is hexagonal without the olfactory bulbs and the paraflocculi, and it is clearly longer than wide (Table 1). Only one sulcus is present on each side of the dorsal surface; this brain is thus regarded as lissencephalic. In ventral view (Fig. 5c-d), the two promontoria of the petrosal bones leave a huge depression on the endocranial cast: they occupy a large surface of the rhombencephalic surface (Table 1). In Chiroptera, the promontorium is very thin and the depression left by the promontorium on the endocast would approximate the imprint of the basal turn of the cochlear canal (see Fig. 5c-d). In *Pa. oltina*, the plane of the basal turn is slightly tilted dorsally relative to the median part of the rhombencephalon. In lateral view (Fig. 5e-f), the general shape of the endocast is rather elongated (especially relative to height, Table 1) with the different components almost aligned. There is only a very subtle angle between the ventral planes of telencephalon and metencephalon, with a cephalic flexure of 171° (Table 1). However, the foramen magnum is not aligned with the posterior part of the brain (it does not open strictly posteriorly), and is tilted ventrally with a cervical flexure of 150° (Table 1).

Telencephalon

In dorsal view (Fig. 5a-b), the olfactory bulbs are ovoid-shaped, antero-posteriorly elongated. They are distinct but still linked longitudinally on their whole length, and separated from the rest of the telencephalon by a short circular fissure of constant width. In lateral view (Fig. 5e-f), they show a lateral bulge distinct from the principal swelling, located posteroventrally. This postero-ventral

bulge/swelling cannot be identified as the olfactory tubercle as its expected location would be more posterior to the olfactory bulbs. Overall, these olfactory structures represent 2.9% of the total volume of the endocast (Table 1). The circular fissure separates the olfactory bulbs from the cerebral hemispheres. It is a little bit tilted anteriorly (Fig. 5e-f and Table 1), and slightly visible in ventral view (Fig. 5c-d). These hemispheres have a pear shape in dorsal view (Fig. 5a-b), with a rounded anterior margin, and their maximal width is reached just before their posterior edge. They do not contact each other and are separated by a broad longitudinal fissure. Their posteromedial corners form obtuse angles. In lateral view (Fig. 5e-f), the posterior part is inflated, with a bigger height than the anterior part, and it occupies grossly the two-thirds of the surface. Such an inflation could correspond to a large hippocampus. The pyriform lobes are small and positioned posteriorly, at the same level as the highest point of the hemisphere (which reinforces the visual impression of a posterior inflation). If they are easy to locate, their dorsal margin is rather difficult to define.

In lateral view (Fig. 5e-f), the rhinal fissure is difficult to identify on its entire length. Its rostral part is rather clear: it starts anteriorly from a dorsal position, just posterior to the circular fissure, then it dives ventrally with a steep slope initially and then with a gentle slope. At its mid-length, it becomes difficult to spot: it passes dorsal to the pyriform lobe (see ESM1: Fig. SI. 5a) but, as they are difficult to delineate dorsally, it is impossible to determine if the rhinal fissure raises posteriorly or not. As the rhinal fissure is not clearly defined on its entire length, the neocortex/paleocortex limit cannot be accurately located, and the neocortical ratio cannot be calculated. The orbitotemporal canal is well visible in dorsal (Fig. 5a-b) and lateral (Fig. 5e-f) views. Its anterior extremity is as the same level as the anterior extremity of the rhinal fissure. It is located rather laterally (Fig. 5a-b) and opens just above the circular fissure (Fig. 5e-f). It has a marked angle in both views, with an anterior part a bit shorter than the posterior one: in dorsal view (Fig. 5a-b), both canals seem anteriorly parallel then posteriorly divergent (more than the borders of the telencephalon). There is a clearly visible sulcus on the neopalleal surface (Fig. 5a-b and e-f): it has a curved path, marked but not very deep. In dorsal view (Fig. 5a-b), the sulci converge posteriorly then start to be parallel. In lateral view (Fig. 5e-f), the curved shape of the path is parallel to the anterior border, and in fact it delineates the anterior border of the inflated posterior part of telencephalon. There is also, ventrally, a short and shallow ramus of this sulcus, with a diagonal orientation (toward the anteriormost and steep part of the rhinal fissure). The first short and shallow ramus is thought to be the pseudosylvia: it seems linked to the rhinal fissure and extends posterodorsally. The second larger sulcus is located more dorsomedially; it is a suprasylvia. Both sulci, linked continuously, form therefore a sylvia. The endocast lacks other sulci: there is no lateral sulcus (there are no sulcus medial to the sylvia) or coronal sulcus (no sulcus more anteriorly). However, the sylvia is marked enough to separate an anterior and a posterior part in the neopallium, which are identified as the reuniens lobe and the arcuate lobe, respectively. The reuniens lobe protrudes a bit, but is clearly shorter than the arcuate one (i.e., the sylvia has a very anterior position).

Diencephalon

Dorsally (Fig. 5a-b), the cast of the epiphysis is visible. It is close to the sagittal plane, located at the level of the posterior margin of the cerebral hemispheres, anterior to the transverse sinus. This cast is quite small in size.

Ventrally (Fig. 5c-d) is the cast of the hypophysis. It is clearly longer than wide (Table 1), with a subtriangular shape. It is located just anterior to the deep casts of the two promontoria, and its anterior margin is at the level of the posterior (narrowest) part of the sphenorbital fissure.

Mesencephalon

The tectum of the mesencephalon (Fig. 5a-b) is fully exposed, without overlap by the telencephalon and/or the metencephalon. The four corpora quadrigemina are exposed. The rostral colliculi, located posterior to the transverse sinus, are very low and hardly distinguishable. They are close to each other. The caudal colliculi are by far larger and prominent, located just posterior to the rostral ones. Contrary to the latter, they are widely separated. They are bulbous, ovoid in shape, and with their long axis almost medio-laterally oriented. In lateral view (Fig. 5e-f), the mesencephalon lies in a shallow valley between telencephalon and metencephalon.

Metencephalon

Dorsally (Fig. 5a-b), the metencephalon is the widest region of the braincase due to the lateral protrusion of the paraflocculi; even without these structures, the cerebellum is still nearly as wide as the cerebrum (Table 1). It is almost twice as wide as long (Table 1). The vermis (Fig. 5a-b and e-f) is almost twice longer than wide in this view, but it is nevertheless quite wide (Table 1). Its anterior part barely reaches the caudal colliculi and shows a small enlargement (Fig. 5a-b). Its posterior part bears three sulci (Fig. 5a-b and g-h), two deep and one shallower, and, contrary to the anterior end, it displays a sizable enlargement. It is difficult here to distinguish the lobules VI and VII A: there only is a slightly flatter section; it is not a groove so it cannot be identified as a VI-VII sulcus, but these part seems to be distinguishable (even if it is not sure). Other parts, however, are more easy to separate: the most anterior groove is here identified as the VII sulcus, with anteriorly the folium vermis and posteriorly the tuber vermis, the median one should be the prepyramidal fissure with the pyramis posteriorly, and the posterior one should be the secondary fissure (even if it is the shallowest of the three), with the uvula posteriorly. Another possibility, relying on the depth of the grooves (Fig. 5e-h), could be to interpret the two deepest grooves (the anterior and median ones) as the prepyramidal and secondary fissures (as a fissure should be deeper than a sulcus) respectively, with therefore the uvula posteriorly and the tuber vermis anteriorly, and the posterior one as an “internal” sulcus of the uvula (which would be more logical as it is the shallowest of the three sulci). The slightly flatter part of the vermis located anterior to the pyramis could be the sulcus VI-VII, separating the lobules VI, VII, and VIII in parts of subequal length, or the sulcus VII. We consider that it is unlikely that a sulcus internal to a lobule is present when sulci separating lobules are absent; we therefore identify the three grooves on the vermis as the VII sulcus, the prepyramidal fissure, and the secondary fissure. The cerebellar hemispheres (Fig. 5a-b and e-f) are clearly separated from the vermis and are positioned more anteriorly relative to it (Table 1). Each of these hemispheres bears two sulci of close depth and length, one anteriorly located (the anterocrural sulcus) and one in a median position (the intercrural sulcus). The paraflocculi are best viewed in ventral view (Fig. 5c-d), where they have an irregular rounded shape (Table 1). They represent 2.3% of the total endocast volume (Table 1). They bear a groove delineating their anteromedial corner, the ventral sulcus of the paraflocculus, which is at its deepest in its central part (which is more or less the central point of the ventral face of the paraflocculi). In dorsal view (Fig. 5a-b), they are partially visible below the cerebellar hemisphere and they show a lateral, small but deep, depression.

The pons-medulla oblongata continuum is exposed in ventral view (Fig. 5c-d), being rather long and wide (Table 1), even if it looks narrow relative to the width of the cast of the promontoria of the petrosal bones (Fig. 5c-d).

Cranial nerve exit casts

The anterior margin of the olfactory bulbs shows two potential exits for the olfactory nerve (I) (Fig. 5c-f). A bundle of nerves seems to exit at the anterodorsal extremity of the olfactory bulbs by a short and almost horizontal (antero-posterior) dorsal part, and there are smaller holes for olfactory nerves on the anteroventral surface of the olfactory bulbs (through the cribriform plate). The imprint of the latter is large, tilted anteriorly and has a quadrate/round shape. It occupies roughly the anterior third of the ventral surface of the olfactory bulbs.

The optical nerve (II) exits through the optic canal, whose anterior opening (the optic foramen) is located just posterior to the olfactory bulbs, anterior to the circular fissure (Fig. 5c-d). It is as large as the other single-nerve foramina, being just a bit smaller than the cribriform plate.

The oculomotor (III), trochlear (IV), and abducens (VI) nerves and the ophthalmic branch of the trigeminal nerve (V1) open together in the sphenorbital fissure while the optic and round foramina are individualized (Fig. 5c-d). The sphenorbital fissures are oblong-shaped, elongated antero-posteriorly (Table 1), and in a rather anterior position relative to the cerebrum: their anterior extremity is close to the circular fissure. They are clearly separated but anteriorly convergent, with a slight diagonal orientation; the sphenorbital bridge (between them) is wider posteriorly.

The maxillary branch of the trigeminal nerve (V2) opens independently from the ophthalmic branch, because a round foramen is present. This foramen is located just near the posterolateral corner of the sphenorbital fissure, and is rather small compared to other single-nerve foramina.

The mandibular branch of the trigeminal nerve (V3) opens in a wide and oval-shaped oval foramen. This foramen is located just posterolateral to the round foramen: there is an alignment of the posterolateral corner of the sphenorbital fissure, the round foramen, and the oval foramen. The oval foramen is quite larger than the round foramen, and slightly larger than the optic foramen.

The facial (VII) and vestibulocochlear (VIII) nerves exit the endocranium through the internal auditory meatus of the petrosal bone. The facial nerve goes anterolaterally (Fig. 5c-d) and a bit ventrally (Fig. 5e-f), but the vestibulocochlear nerve goes clearly anteroventrally (Fig. 5e-f). The cochleae are so close to each other in ventral view (Fig. 5c-d) that the casts of these nerves are roughly on the same medio-lateral line as those of the mandibular branches of the trigeminal nerve (V3), which exit through the oval foramina.

The glossopharyngeal (IX), vagus (X), and accessory (XI) nerves exit through the jugular foramen (Fig. 5c-d). It is located just posterior to the two previous nerves, at the same medio-lateral level. This foramen is of large size, as three nerves pass through. It is coalescent with the basicochlear fissure, medially.

The hypoglossal nerve (XII) exits through the hypoglossal foramen. It is located a bit more medially than the previous foramina, at the medio-lateral level of the round foramen, and between the jugular foramen and the foramen magnum anteroposteriorly (it opens in the ventral condyloid fossa, comprised in the exoccipital). It is of medium size relative to other single-nerve foramina.

Other braincase opening casts

The cast of the ethmoidal foramen (Fig. 5e-f) is present on both sides and is rather wide. It is located, on the endocast, on the lateral face of the olfactory bulb, in a posteroventral position. It is

however difficult to spot this foramen without the skull (i.e., on a natural endocast) as it is shallow (ESM1: Fig. SI. 6a).

The casts of the pyriform (piriform) fenestra, of the carotid foramen, and of the basicochlear fissure are visible on the endocast (Fig. 5c-d), coalescent, and surrounding the petrosal bone anteriorly and medially. These three openings join the jugular foramen, posteromedial to the petrosal bone.

The foramen magnum (Fig. 5c-d and g-h) is rather wide (Table 1), almond-shaped. It is located just ventral to the posterior part of the cerebellum, its anterior margin lying posterior to the casts of the promontoria. This foramen is tilted ventrally (Table 1), opening posteroventrally.

Comparisons with other hipposiderid fossil endocasts

Overall shape

The specimen of *Pa. quercyi* is a well-preserved cranium filled with clay matrix, only a small portion of its cranial vault is broken. Despite the presence of sediment in the braincase, the endocranial cast has been satisfactorily virtually extracted (Fig. 6b, f and i, and ESM1: Fig. SI. 2b and f, Fig. SI. 3b, f and i and Fig. SI. 4b, f and i) and has a total volume of 364.6 mm^3 (Table 1). The specimen of *H. (Ps.) schlosseri* is a natural endocranial cast partly embedded in a phosphatized clay matrix with dorsal and both lateral surfaces exposed (Fig. 6c and j, and ESM1: Fig. SI. 2c and g, Fig. SI. 3c and j and Fig. SI. 4c and j), but its ventral surface could not be virtually segmented; this aspect of the cranium therefore remains undescribed for this species, and the total volume of the braincase could not be estimated. This specimen is morphologically similar to those figured with very low details by Yao et al. (2012). The natural endocranial cast of *H. (Ps.) bouziguensis* is also partly embedded in the sediment and its ventral surface, not directly accessible, was extracted virtually (Fig. 6d, g and k, and ESM1: Fig. SI. 2d and h, Fig. SI. 3d, g and k and Fig. SI. 4d, g and k). Except for the petrosals, which are missing, the whole surface of the endocast of this taxon is well preserved and the volume of the braincase has been estimated of 435.2 mm^3 (Table 1). This specimen is also morphologically close to those figured by Yao et al. (2012), especially their specimen 3. Overall, specimens figured here are very similar to and of better quality than those of Yao et al. (2012); we thus do not include the latter in our comparisons. The four specimens show the same global shape (Fig. 6a-d): they are hexagonal, longer than wide (Table 1), with a single neocortical sulcus (shallower in *Pa. quercyi*, deeper in *H. (Ps.) bouziguensis*) and thus lissencephalic. In ventral view (Fig. 6e-g), endocasts of *Pa. quercyi* and of *H. (Ps.) bouziguensis* also resemble that of *Pa. oltina*, with petrosals occupying a large surface of the posterior part (Table 1), and with roughly the same pattern of basicranial foramina. In lateral view (Fig. 6h-k), the global scheme of all taxa described here is also very close. There are however some differences: (1) the telencephalon of *H. (Ps.) bouziguensis* is more inflated dorsally than the three others, (2) *Pa. quercyi* and *H. (Ps.) schlosseri* have a flatter reuniens lobe compared to *Pa. oltina* and *H. (Ps.) bouziguensis*, (3) the general position of the orbitotemporal canal cast on the telencephalon is clearly more ventral in *H. (Ps.) bouziguensis* than in the three others, and (4) the orientation and relative size of olfactory bulbs varies between taxa. The cephalic and cervical flexures are of a similar magnitude for all specimens (Table 1); the relative organization of brain sub-structures is the same across these taxa. The specimen of *H. (Ps.) bouziguensis*, compared to the three others, gives a visual impression of a slight antero-posterior compression (Fig. 6h-k), but has comparable height/length ratio for the endocast as a whole, for the cerebrum, and for the cerebellum relative to the other species (Table 1). Cephalic flexures vary a bit between the three species for which it could be measured: *Pa. oltina* has the largest value, *Pa. quercyi*

an intermediate value, and *H. (Ps.) bouziguensis* has the acutest angle (Table 1). There are also differences in the angle between the circular fissure and the foramen magnum between species, *Pa. oltina* having the most acute one (Table 1). In fact, *Pa. quercyi* has a more ventrally tilted circular fissure than *Pa. oltina*, and *H. (Ps.) bouziguensis* has a much more ventrally tilted foramen magnum (Table 1).

Telencephalon

In dorsal view (Fig. 6a-d), the general shape of the olfactory bulbs is close for all fossil hipposiderid taxa but there are some subtle differences. The olfactory bulbs of *Pa. quercyi* and of *H. (Ps.) bouziguensis* are similar in shape and size to those of *Pa. oltina*, but they are closer to each other in *Pa. quercyi* and even more in *H. (Ps.) bouziguensis*. The olfactory bulbs of *H. (Ps.) schlosseri* are narrower than those of the three other taxa. In lateral view (Fig. 6h-k), each specimen differs from the other. Compared to *Pa. oltina*, the three other extinct hipposiderid taxa present olfactory bulbs that are pointing anteriorly, and not dorsally raised. *Palaeophyllophora quercyi* has the longest and biggest olfactory bulbs relatively to the whole endocast (3.2% of total volume; Table 1). Both specimens of *Hipposideros (Pseudorhinolophus)* have shorter and dorsoventrally larger olfactory bulbs, with a rounder shape, those of *H. (Ps.) schlosseri* being smaller than those of *H. (Ps.) bouziguensis*. The olfactory bulbs of the described species of *Hipposideros (Pseudorhinolophus)* are globally smaller than those of *Palaeophyllophora* (2.6% of total volume in *H. (Ps.) bouziguensis*). The lateral bulge observed in *Pa. oltina* is also present in the other three specimens but it is smaller. In *Pa. quercyi*, this swelling is weakly developed but present, while in *H. (Ps.) schlosseri*, it is well visible in spite of the smaller size of the olfactory bulbs. In *H. (Ps.) bouziguensis*, the lateral swelling has a large lateral extent similar to *Pa. oltina*, but its distinction relative to the main part of olfactory bulbs is smoother. The shape of the circular fissure of the two *Hipposideros (Pseudorhinolophus)* and of *Pa. quercyi* is similar to *Pa. oltina*. In dorsal view (Fig. 6a-d), the cerebral hemispheres of the fossil hipposiderids described here have the same pear-shape and a maximal width reached rather posteriorly. However, there are some differences in how they contact each other as well as on the shape of their posteromedial corner. In *H. (Ps.) bouziguensis*, the interhemispheric gap is the narrowest, the two cerebral hemispheres are closer to each other on a longer distance; their posteromedial corner is almost right, the least obtuse of all specimens. In other taxa described here, the interhemispheric gap is wider and the posteromedial corner is more opened. In *H. (Ps.) schlosseri*, the gap between cerebral hemispheres is a bit wider than in *Pa. oltina* but it is constant, while it is narrower anteriorly and widens posteriorly in *Pa. oltina*. This gap between cerebral hemispheres is even wider in *Pa. quercyi*: the interhemispheric gap, rather wide posteriorly (as *Pa. oltina* and *H. (Ps.) schlosseri*), is wider anteriorly. However, the medial margin of the reuniens lobe is blurry (maybe due to preservation) and the anterior width of the gap between the hemispheres is difficult to assess. Laterally (Fig. 6h-k), there are different degrees of inflation of the reuniens and arcuate lobes among species. Both lobes are much inflated in *H. (Ps.) bouziguensis*, a bit more than in *Pa. oltina*. In *Pa. quercyi* especially, but also in *H. (Ps.) schlosseri*, the reuniens lobe is less inflated. The cerebrum of *H. (Ps.) bouziguensis* appears to be more antero-posteriorly compressed; this could be a visual artefact due to its more dorsoventral global inflation. Laterally (Fig. 6h-k), the pyriform lobes are located a bit more posteriorly in *Palaeophyllophora* than in *Hipposideros (Pseudorhinolophus)*. They are located at, or just a bit posterior to, the summit of the arcuate lobe in the former, while they are a bit anterior to it in the latter. The development of the pyriform lobe follows that of the arcuate lobe (they are the most developed in *H. (Ps.) bouziguensis*), and they are a bit more salient in *H. (Ps.) schlosseri* than in *Palaeophyllophora* specimens. The ventral view (Fig. 6e-g) does not show any other difference of these lobes between taxa.

Laterally (Fig. 6h-k), on all specimens, the rhinal fissure is difficult to identify. Its anterior part is less visible in *Pa. quercyi* than in other specimens. Its posterior part is decipherable on the *Pa. quercyi* and *H. (Ps.) schlosseri* specimens: there is a subtle ridge delineating the dorsal margin of the pyriform lobe in anterior view (ESM1: Fig. SI. 5) that is continuous with the anterior part of the rhinal fissure observed in lateral view (Fig. 6h-k). This ridge could mark the location of the posterior part of the rhinal fissure, and it is also distinguishable in the other specimens (Fig. 6h-k; ESM1: Fig. SI. 5). This posterior part is best seen (through the ridge) in lateral view on the *Pa. quercyi* specimen (Fig. 6h-k). On its whole length, the course of the rhinal fissure is roughly the same in all specimens with its posterior third strongly dorsally tilted. The orbitotemporal canal, visible on all specimens, shows differences between taxa. In lateral view (Fig. 6h-k), it is located more ventrally in *H. (Ps.) bouziguensis*, especially its anterior part, which is more ventrally flexed. In *Pa. quercyi*, the posterior part is difficult to track, but the dorsalmost angle of the canal is located more dorsally than in other specimens, suggesting a general more dorsal position. In *H. (Ps.) schlosseri*, the position of this canal is similar to *Pa. oltina*. In dorsal view (Fig. 6a-d), *H. (Ps.) bouziguensis*, again, differs markedly from the other hipposiderid taxa with a more lateral location of the orbitotemporal canal. Other specimens show a similar, more medial, position of the orbitotemporal canal. That of *Pa. oltina* is a little bit more lateral than the two others. The dorsal inflection of this canal is less acute in both *Hipposideros (Pseudorhinolophus)* taxa than in both *Palaeophyllophora* ones. The sylvia is visible on all specimens, roughly at the level of the second quarter (antero-posteriorly) of the cerebrum (Fig. 6a-d and h-k). In lateral view (Fig. 6h-k), it is shallow in *Pa. quercyi*, a bit deeper in *Pa. oltina* and in *H. (Ps.) schlosseri*, and it is the deepest in *H. (Ps.) bouziguensis*. The pseudosylvia seen in *Pa. oltina* is found only in *H. (Ps.) schlosseri* where it is very short. This sulcus is lacking in the other taxa of the sample. In dorsal view (Fig. 6a-d), the sylvia is shallow posteriorly for *Pa. oltina* and *H. (Ps.) schlosseri* (it is always shallow for *Pa. quercyi*). However, in *Pa. oltina*, there is a slight posterior extension of the sylvia (the posterior extension of the suprasylvia) marked by a terminal angle. In *H. (Ps.) bouziguensis*, the sylvia is deeper and its posterior extension is present, clearer than in *Pa. oltina*.

Diencephalon

In dorsal view (Fig. 6a-d), the delineation of the cast of the epiphysis of the fossil hipposiderid taxa described here is rather unclear. However, imprints of all expected structures on the dorsal surface between cerebrum and cerebellum (i.e., epiphysis cast, transverse sinus, rostral and caudal colliculi) in *Pa. oltina* allow us to identify and locate these different structures in all taxa. This cast is small and hardly distinguishable in both *Palaeophyllophora* species; it is even smaller in the *Hipposideros (Pseudorhinolophus)* ones.

In ventral view (Fig. 6e-g), the hypophysis is well preserved in all specimens (when ventral view is preserved). In *H. (Ps.) bouziguensis*, the hypophysis cast is similar to that of *Pa. oltina*: it is of subtriangular shape, longer than wide (Table 1), and in the same position. It is however a bit less protruding ventrally. In *Pa. quercyi*, it is wider than long (Table 1), ovoid in shape.

Mesencephalon

The tectum of the mesencephalon (Fig. 6a-d) is fully exposed in all specimens. The rostral colliculi are distinguishable in *Pa. oltina* and in the two *Hipposideros (Pseudorhinolophus)* specimens; their corresponding area is poorly preserved on the *Pa. quercyi* specimen. In *H. (Ps.) bouziguensis*, they have a shape similar to those of *Pa. oltina*. In *H. (Ps.) schlosseri*, there is rather a plateau, with the two

little prominences of the rostral colliculi. These rostral colliculi are also a bit higher (Fig. 6h-k) than in *Pa. oltina*, but they are also more difficult to distinguish. The caudal colliculi are clearly visible: their long axis is diagonally oriented, and they are more elongated in *Pa. oltina* and *H. (Ps.) bouziguensis* than in *Pa. quercyi* and *H. (Ps.) schlosseri*. Moreover, they are more separated in *Pa. quercyi* than in other fossil hipposiderid taxa. Laterally (Fig. 6h-k), the tectum of the mesencephalon lies in a shallow valley between the cerebrum and the cerebellum. The two latter structures are, however, of different heights depending on the taxa. The cerebrum and cerebellum are the highest in *H. (Ps.) bouziguensis*, where the tectum lies in a clear depression; they are a bit lower and the tectum lies in a shallower depression in *Pa. oltina*, *Pa. quercyi*, and *H. (Ps.) schlosseri*. In *H. (Ps.) bouziguensis*, despite the fact that the mesencephalon is more depressed, the caudal colliculi are clearly the most protruding; those of other taxa are of a similar, less protruding, degree of prominence.

Metencephalon

In dorsal view (Fig. 6a-d), the metencephalon is the widest region of the braincase for *Pa. quercyi* and for *Pa. oltina*; the lack of preservation of the paraflocculi in the other taxa does not allow us to confirm this for *Hipposideros (Pseudorhinolophus)* specimens. Yet, in all specimens, the width of the cerebellum is twice its length, nearly as wide as the cerebrum (Table 1). The vermis is also quite wide (a bit larger in *Pa. oltina* than in others), but still longer than wide (the longest in *H. (Ps.) bouziguensis*, Table 1). In all specimens, as for *Pa. oltina*, it enlarges posteriorly and a bit anteriorly, almost reaching the caudal colliculi anteriorly. The anterior margin of the vermis is much more delineated in *Hipposideros (Pseudorhinolophus)* species than in *Palaeophyllophora*. In lateral view (Fig. 6h-k), the vermis is a bit higher in *Palaeophyllophora* species and in *H. (Ps.) bouziguensis* than in *H. (Ps.) schlosseri*. Moreover, the shape of the dorsal surface of the vermis in this view is more convex in *H. (Ps.) bouziguensis* than in *Palaeophyllophora* species and in *H. (Ps.) schlosseri*. The surface of the vermis of *Pa. quercyi* does not show any sulcus, but the preservation is poorer than in other specimens. There is a VII sulcus and a prepyramidal fissure in all three other species (Figs. 5g-h and 6a-d and h-k). There also is a secondary fissure on the occipital face of the vermis surface of *Pa. oltina* and *H. (Ps.) bouziguensis*. In the latter species, there even is a VI-VII sulcus: it is shallow but present, visible in both dorsal and lateral views (Fig. 6a-d and h-k). It divides the VI and VIIa lobules inequally, the declive (VI) being much longer (more than the half of the vermis length in dorsal view, Fig. 6a-d). The cerebellar hemispheres (Fig. 6a-d) of *H. (Ps.) schlosseri* are narrow, not protruding laterally, and the intercrural sulcus is hardly distinguishable, while the hemispheres have the same general shape and the intercrural sulcus is marked in other specimens. The vermis is protruding posteriorly in *Pa. oltina* and in *H. (Ps.) schlosseri*, a bit less in *Pa. quercyi*, and it protrudes the least in *H. (Ps.) bouziguensis*. Concurrently, the cerebellar hemispheres are more anteriorly located relative to the vermis in the two former species; in dorsal view, they have a greater antero-posterior overlap between vermis and cerebellar hemispheres (Table 1). The paraflocculi have been only preserved in *Palaeophyllophora* specimens (Fig. 6e-g), where they are of close morphology, but they are a bit larger in *Pa. oltina* than in *Pa. quercyi* relatively to the whole endocast (2.3% vs 1.8% of the total volume; Table 1). In dorsal view (Fig. 6a-d), the paraflocculi of *Pa. oltina* are more visible than those of *Pa. quercyi*. In *Pa. quercyi*, the paraflocculi are located more medially: they protrude less laterally (Fig. 6a-d) and, in ventral view (ESM1: Fig. SI. 4e-g), “necks” of the paraflocculi (the part linking them to the rest of the metencephalon) are not visible (they are for *Pa. oltina*). The medial part of the paraflocculus (Fig. 6e-g) protrudes a bit posteriorly in *Pa. quercyi*, while the lateral one protrudes posteriorly in *Pa. oltina*. The ventral sulcus of paraflocculus is less marked in *Pa. oltina* than in *Pa. quercyi* (ESM1: Fig. SI. 4e-g),

but it could also just be a matter of preservation. In lateral view (ESM1: Fig. SI. 4h-k), the lateral depression present in *Pa. oltina* is absent in *Pa. quercyi*.

The pons-medulla oblongata continuum (Fig. 6e-g) is longer than wide in all specimens (Table 1), and relatively longer in *Pa. quercyi* than in the two other specimens. Otherwise, there are no clear differences between taxa.

Cranial nerve exit casts

The olfactory nerve exit pattern is generally similar across specimens (Fig. 6e-k). Yet, some differences occur regarding the olfactory nerves exit (imprint of the cribriform plate + dorsal bundle of nerves). It varies in terms of orientation and of extension: it is more tilted anteriorly in *Pa. oltina* than in other taxa, and forms a large surface in *Pa. oltina* and *H. (Ps.) bouziguensis* while it is of intermediate dimensions in *Pa. quercyi* and consists of a small and rounded surface in *H. (Ps.) schlosseri* (Fig. 6e-g and ESM1: Fig. SI. 5). Optic foramina (Fig. 6e-g) are separated from the sphenorbital fissure in all specimens, but their position varies. They are at the posterior end of olfactory bulbs in *Palaeophyllophora* specimens (optic canals are even visible in *Pa. quercyi*), at the level of the circular fissure. Optic foramina are more anteriorly located in *H. (Ps.) bouziguensis*, being at the middle of the olfactory bulbs, just posterior to the imprint of cribriform plate. The structures identified here as optic foramina in *H. (Ps.) bouziguensis* are rather unusually located (ventral aspect of the olfactory bulbs) and very dissimilar on the left and right sides of the specimen. Their shape and size are roughly similar to those of *Pa. oltina* and they are a bit posteriorly located to the imprint of cribriform plate. Another possibility for optic foramina identification could be the small notches at the anterior end of each sphenorbital fissure; optic foramina would therefore be confluent with these fissures. In this case, compared to *Palaeophyllophora* specimens, the position of the optic foramina would be similar but their shape would be very different. The sphenorbital fissures (Fig. 6e-g) are similarly located ventral to the anterior part of cerebrum in all specimens. They are however located a bit more anteriorly in *H. (Ps.) bouziguensis* than in *Palaeophyllophora*, the former bearing a small anterior notch at the level of the circular fissure. They are also a little bit longer and a bit more apart in *Palaeophyllophora* specimens (Table 1). Otherwise, on the three specimens, the sphenorbital fissures are roughly oblong-shaped, rather large (especially relative to the gap between them), and converge anteriorly. Round and oval foramina are individualized on the three specimens. In all three specimens, the round foramen is clearly smaller than the oval one, which is rather large, round-shaped to oval-shaped. The position of the oval foramen is also similar, located posterolateral to the sphenorbital fissure. The position of the round foramen, however, varies: it is located between the sphenorbital fissure and the oval foramen in *Pa. oltina* (all three structures being juxtaposed and aligned), while it is lateral to the posteriormost part of the sphenorbital fissure in *Pa. quercyi* and posterior to it with a marked gap in *H. (Ps.) bouziguensis*. There are no differences regarding the exits of facial and vestibulocochlear nerves and the cast of the jugular foramen among the two *Palaeophyllophora* specimens (petrosal is not preserved in *H. (Ps.) bouziguensis*), in terms of size and orientation (Fig. 6e-k) for the two former, and in terms of size, shape, and location for the latter (Fig. 6e-g). The size, shape, and location of the hypoglossal foramen are similar across the three specimens where it is preserved; it lies in a slight more medial position in *Pa. quercyi* (Fig. 6e-g).

Other braincase opening casts

The ethmoidal foramen is at the level of the lateral swelling of the olfactory bulbs in both *Palaeophyllophora* species (this is confirmed by cranial observation, ESM1: Fig. SI. 6a-b). This foramen is however tough to decipher without the skull (i.e., based on natural endocast); we thus consider that its location is similar in *Hipposideros (Pseudorhinolophus)* species (ESM1: Fig. SI. 6c-d), but this cannot be confirmed yet. Comparing apertures surrounding the petrosal imprint (Fig. 6e-g; i.e., pyriform fenestra, carotid foramen, and basicochlear fissure) of the *H. (Ps.) bouziguensis* specimen is difficult as only their lateral side is preserved (as for the jugular foramen). In both *Palaeophyllophora* specimens, the three previously mentioned structures plus the jugular foramen are confluent. The cast of the basicochlear fissure is thicker in *Pa. oltina*, and the pyriform fenestra cast is more lateral in *Pa. quercyi* (Fig. 6e-g). The foramen magnum is very similar in size, shape, and orientation between *Palaeophyllophora* specimens. In *H. (Ps.) bouziguensis*, the foramen magnum bears an anterior notch and opens more ventrally than in the three other taxa (Fig. 6h-k and Table 1). It therefore has a different shape and size in ventral view (Fig. 6e-g): its anterior outline is angular and its posterior one is curved.

Common endocast measurements

Encephalization quotient

The encephalization quotient corresponds to the ratio between the observed brain mass of an organism and the expected brain mass of this organism given its body mass (Jerison 1973; van Dongen 1998). EQ values, brain and body masses of the described species are provided in Table 2, and the boxplots of EQ values of mammals through Tertiary epochs and of extant species are presented Fig. 7 and ESM1: Fig. SI. 7 (following Eisenberg and Wilson (1978) and Jerison (1973) formulas respectively). As previously described in the literature (e.g., Jerison 1973), a general increase of EQ values from Paleocene to Oligocene is observed in mammals; however, this is not true for hipposiderid bats, whose EQ values remain relatively constant through time. This is supported by Kruskal-Wallis tests of the EQ comparing these epochs: there is at least a difference between epochs in mammals (Table 3), especially around the Eocene/Oligocene boundary (Table 4 and ESM2: Table SI. 6), but not in bats (here only represented by hipposiderid for fossils species; Tables 5 and 6 and ESM2: Table SI. 6). In hipposiderids only, there is a slight significance of both Fisher and Kruskal-Wallis tests (Table 3 and ESM2: Table SI. 6) and there is a slight tendency to a difference between Eocene and extant hipposiderids (Table 6 and ESM2: Table SI. 6), but p-values are superior or close to the 5% alpha risk. Interestingly, extant bats, and especially extant hipposiderids, are in the lower part of mammal EQ values (overlapping the lower whisker of the general boxplot; Fig. 7 and ESM1: Fig. SI. 7), whereas EQ values of fossil hipposiderid bats were closer to central global mammalian values in the Eocene. This suggests that hipposiderid EQ apparently did not increase through time, contrary to non-bat mammals in general.

A complementary way to illustrate the EQ is to plot the log brain mass vs the log body mass with the regression lines derived from the EQ formulas of Eisenberg and Wilson (1978) and of Jerison (1973) for all mammals and for bats only (ESM1: Fig. SI. 8). As illustrated previously (Fig. 7) and statistically tested (Table 4 and ESM2: Table SI. 6), this figure (ESM1: Fig. SI. 8) shows a bump over the regression lines (i.e., in the encephalization) of the “other mammals” convex hull at the Eocene-Oligocene transition. Bats, on the other hand, are under the Jerison (1973) regression line and at the level of the Eisenberg and Wilson (1978) regression line, without clear difference between extant bats and Eocene to Miocene ranging bats (Tables 5 and 6 and ESM2: Table SI. 6).

Olfactory bulbs and paraflocculi volumes relative to brain volume

Olfactory bulbs and paraflocculi are quite prominent in bat brains (see Baron et al. 1996) and in fossil species described here (Figs. 3-6 and ESM1: Figs. SI. 2-4). The volume of these two structures relative to brain volume is commonly mentioned in the literature (e.g., Jerison 1973; Ramdarshan and Orliac 2016; Bertrand et al. 2018a, b, 2019). We plotted natural logarithms of each volume against the logarithm of brain volume, which allows to take into account the potential effect of allometry and to compare extreme points. Regarding olfactory bulbs, we compared our fossil hipposiderid species to bats in general, but also more specifically to other rhinolophoids and to other hipposiderids. In the biplot illustrating this relationship (Fig. 8a), our fossil sample falls roughly in the middle of all extant bats cloud of points. Pteropodids have the highest values, as they are generally bigger bats ("megabats"). Rhinolophoids and hipposiderids have a wide morphospace but also fall roughly in the middle of all "microchiropteran" bats (i.e., Yangochiroptera + Rhinolophoidea); fossil hipposiderid taxa fall in hipposiderids. Regarding parafloccular volume compared to endocranial volume (Fig. 8b), the morphospace of mammals is quite large, that of bats and of other laurasiatherians too. For rodents, both extinct and extant data are available: extinct species cluster together and overlap the morphospace of modern representatives. Concerning bats, the two fossil species are close to each other and to modern bat species (especially, *Pa. quercyi* falls very close to the rhinolophoid *Rhinolophus ferrumequinum*). "Microchiropteran" bats lie in the lower part of the biplot, which is expected given their smaller size; yet, they do not show extreme values compared to other mammals, despite of their particular locomotor behavior.

Discussion

Brain vs endocranial cast external morphology in Hipposideridae

Among mammals, some differences in the degree of similarity between the brain and the endocast are observed. For instance, Dechaseaux (1962) showed that, in sheep, the cranial endocast reflects well the morphology of the brain, which is not the case in cetacean and proboscideans, mostly due to the presence of meningeal tissues and/or blood vessels between the brain and the dorsal part of the braincase (e.g., dura mater, rete mirabile). In the literature, Insectivora, Chiroptera, and Carnivora are considered to show the highest correspondence between the endocranial cast and the external shape of the brain (Orlov 1961; Dechaseaux 1962; Kochetkova 1978). Paleoneurology is therefore promising, though limited and needs to be coupled with a detailed knowledge of the brain of extant species (Dechaseaux 1962; Neubauer 2014). This aspect is still patchy regarding bats, and especially Hipposideridae (see Baron et al. 1996 for the latest review at the Chiroptera scale), which makes morphological comparisons between extant and extinct species not straightforward. Only few hipposiderid brains have been macromorphologically described in the literature (one figure and a family-level general description in Baron et al. 1996) and no comparison of the external morphology of brain vs endocranial cast have never been realized for the family – or at the ordinal scale.

Another issue regarding the comparison between extinct and extant bat brains is that the phylogenetic relationships within Chiroptera has drastically evolved since the major works on extant bats of Baron et al. (1996) (e.g., bats placed in Laurasiatheria rather than in Euarchontoglires, Mega-/Microchiroptera vs Yinptero-/Yangochiroptera; see Simmons and Geisler (1998), Simmons (2000), and Jones et al. (2005) for reviews) and brain characteristics proposed for different bat families have to be revised because of the changes in their taxonomic content. For instance, Baron et al. (1996) defined

the general brain characteristics of Hippposideridae based on a taxonomic sample including species that are nowadays placed in a different family (*Triaenops persicus*, now placed in the Rhinonycteridae).

When compared to the brain of the modern *Hipposideros diadema* figured by Baron et al. (1996:figs.8,24,40; Fig. 9), the cranial endocasts of the present fossil sample (Fig. 6 and ESM1: Figs. SI. 3-4) appear to reflect well the external morphology of the brain of extant hipposiderid in dorsal and lateral views. The main differences concern: (1) the precision of the folding of the cerebrum and the cerebellum (neocortical foldings are more marked on the brain; more foldings are visible on the vermis and on the cerebellar hemispheres on the brain); (2) the exact delineation of the midbrain region (there are imprecisions on an endocast regarding the posterior extent of the cerebral hemispheres and the anterior extent of cerebellar hemispheres); (3) the exposure of the mesencephalic colliculi (rostral colliculi are less visible and less delineated on an endocast); and (4) the presence of blood sinuses/vessels and other nervous structures that can obscure some brain parts and overestimate its size (e.g., Balanoff and Bever (2017) for a general review, and Benoit (2015) for how to account for this aspect in proboscideans).

In ventral view, there are major differences that mainly concern nerve pathways and exits. On endocasts, the cranial nerve pattern and blood vessel pathways can mainly be reconstructed via the foramina and fissures that pierce the different bones of the braincase (e.g., Muizon et al. 2015). This makes direct comparisons between endocranial cast and brain external morphology difficult. For instance, the shape of the olfactory bulb area differs between brain and endocasts because of the presence of the cribriform plate cast on the latter, making slight overestimation of olfactory bulb volume likely. The most striking difference concerns the optic nerve. On the cranial endocast of our hipposiderids, only the end of the intracranial course of the optic nerve is visible (either by the optic foramina or by the anterior part of the optic canal), and the location of the optic chiasma cannot be determined. On the brain illustrated by Baron et al. (1996), the optic chiasma reveals to be located more posteriorly than the exit of the optic nerve, close to the hypophysis. Another major difference apart from cranial nerve exits concerns the external morphology of the pons-medulla oblongata continuum: it is fully smooth on an endocast, whereas there are more details on the brain. However, these details do not guarantee to distinguish pons from medulla oblongata in other bat brains (Baron et al. 1996: figs. 51-56).

Cursory glance at the hipposiderid brain evolution

The general morphology of endocasts is similar in all four fossil hipposiderid species. They all show a similar morphology of the telencephalon in terms of neocortical fissuration and expansion, and of the general shape of the olfactory bulbs and pyriform lobes. They all exhibit protruding epiphysis and hypophysis, and a widely exposed mesencephalon with large, protruding caudal colliculi and subtle rostral colliculi. In all specimens, the metencephalon is wide, especially the cerebellum, which bears a wide and long vermis, a similar rough shape of cerebellar hemispheres, and large and protruding paraflocculi. The pattern of cranial nerve exits and basicranial foramina is also very conservative within the sample of fossil hipposiderid species described here, with a long sphenorbital fissure neither coalescent with the optic foramen nor with the round foramen. The external morphology of the brain of *H. diadema* as illustrated by Baron et al. (1996) indicates that this extant species also shares the same characteristics. Based on our observations, the general morphology therefore seems to be highly conservative within the hipposiderid family.

Concurrently with this general morphological conservatism through Cenozoic times, there is a stasis in EQ values in hipposiderid bats during the Paleogene/Neogene (Fig. 7 and ESM1: Figs. SI. 7-8). Since Eocene times, the EQ value of mammals generally increased with time (as postulated since Jerison (1973)), but it is apparently not the case in bats: the EQ of Eocene (or Oligocene for *H. (Ps.) schlosseri*) and Miocene hipposiderids is close to that of extant ones (Tables 3 to 6). EQ values of Eocene bats were closer to central values of other mammals, but this gap widened through time because of differential EQ evolution between bats and non-bat mammals. The global stasis in the EQ through time observed here in one chiropteran family may of course overlook mixed patterns of encephalization evolution across bat families. Be that as it may, this uncommon EQ stasis relative to other mammals, exemplified here by Hipposideridae, could be linked to the uncommon ecology of bats: their adaptations for flight and for echolocation (except for pteropodids) may have constrained the range of morpho-anatomo-functional variability of their brain (Safi et al. 2005).

The "principle/law of proper mass" defined by Jerison (1973:9) implies that "the relative masses of neural tissue (…) are related to the relative importance of the functions in the species." In fossil endocast studies, the relative volume of olfactory bulbs cast is generally linked to olfaction and to the importance of the sense of smell relative to other senses such as vision or audition (e.g., Jerison 1973; Takai et al. 2003; Silcox et al. 2009; Rowe et al. 2011; Gonzales et al. 2015; Bertrand et al. 2019). When olfactory bulb volume is plotted against brain volume (log-transformed data; Fig. 8a), the fossil hipposiderid bats fall within the morphospaces of extant bats (that of hipposiderids, rhinolophoids, and bats in general), suggesting a similar importance of olfaction in their behavior (and/or no difference through time). Regarding the paraflocculi, they are linked to the vestibuloocular reflex that stabilizes vision during movements (Ito 1982; Waespe et al. 1983; Paulin 1993; Rambold et al. 2002; Voogd and Wylie 2004). Recent studies used paraflocculi volumes (relying on the subarcuate fossa as a proxy) to discuss the degree of environment complexity during the evolution of sciuromorph rodents, assuming that a complex locomotor environment is related to gaze stabilization and thus large paraflocculi (Bertrand and Silcox 2016; Bertrand et al. 2018a, b). However, based on a sample of birds and mammals, Ferreira-Cardoso et al. (2017) did not find any correlation between parafloccular fossa volume and ecological traits, suggesting that this measure is not a reliable ecological proxy. This studies use a wide sample with few representatives per group, but covers a broad range of ecological traits. Given the assumed role of paraflocculi in spatial movement, and following the principle of proper mass (Jerison 1973), large paraflocculi would be expected in bats given their complex locomotor behavior (3D and aerial environment). According to our results (Fig. 8b), there are no clear difference between bats and other mammals, or when comparing extant and fossil bats.

The general evolution of the macromorphology of our fossil endocasts is therefore congruent with the various measurements mentioned above, suggesting that the main characteristics of the hipposiderid brain are conserved through time. For instance, the prominence of the caudal colliculi clearly indicate a sophisticated echolocation as in extant bats (Baron et al. 1996; Voogd et al. 1998); the large cerebellum, similar to extant species, is also supposedly related to sophisticated echolocation and (at least) powered flight (Paulin 1993). This apparent general stasis in hipposiderid brain characteristics (previously proposed at the Chiroptera scale, but never tested; Dechaseaux 1956; Baron et al. 1996) is congruent with the paradigm that bats adapted very rapidly and very early during their evolutionary history (Simmons and Geisler 1998; Simmons et al. 2008) and then did not change much afterwards, except punctual new optima in some families, which is not the case of Hipposideridae (Amador et al. 2019). Furthermore, the lissencephalic telencephalon (with a limited expansion of the

neocortex) and exposed mesencephalon made the brain of bats generally regarded as plesiomorphic within mammals (Dechaseaux 1956; Edinger 1963). However, these features could in fact be derived conditions (Edinger 1963; Kelava et al. 2013) that would have appeared early in Chiroptera evolution and would have been retained through time since at least the late Eocene given our detailed observations on fossil hipposiderid bats. This also raises questions about the ancestral morphology of bats brains and the very first steps of their evolutionary history.

Thorough examination of the hipposiderid brain

Despite the general conservative morphology of the brain of hipposiderid bats described above, several differences are observed that can be interpreted in terms of phylogeny and/or evolutionary "grades" and/or allometry. Our sample is composed of two groups of two species: *Pa. oltina* and *Pa. quercyi* that belong to the genus *Palaeophyllophora* (Maitre 2014), sister taxon to the genus *Hipposideros* (Ravel et al. 2016; Fig. 1), and *H. (Ps.) schlosseri* and *H. (Ps.) bouziguensis* that belong to the same genus, *Hipposideros*, and to the same subgenus, *Pseudorhinolophus* (Maitre 2014). Differences observed between *Palaeophyllophora* and *Hipposideros* (*Pseudorhinolophus*) species are thus likely to be of phylogenetic interest. *Hipposideros (Pseudorhinolophus)* subgenus has been proposed to be a paraphyletic assemblage of stem species to the extant genus *Hipposideros*, with *H. (Ps.) bouziguensis* diverging earlier than *H. (Ps.) schlosseri* (Ravel et al. 2016; Fig. 1). Therefore, differences distinguishing *H. (Ps.) schlosseri* are also likely to be of phylogenetic interest. A further aspect is that *H. (Ps.) bouziguensis* is more recent than the three other species (i.e., early Miocene vs at least Paleogene, at most late Eocene; Fig. 1), but diverges earlier than *H. (Ps.) schlosseri* (Ravel et al. 2016). Thus, differences distinguishing *H. (Ps.) bouziguensis* from all other three species might be of temporal interest (i.e., "evolutionary grades"). Finally, size also varies a bit in this sample: *H. (Ps.) schlosseri* is the smallest species of our fossil sample, *Pa. oltina* is the largest, and *Pa. quercyi* and *H. (Ps.) bouziguensis* are of close intermediate size; such an ordination of differences is likely to be correlated to size and to be related to allometry.

Characters of potential phylogenetic interest

Several characteristics differentiate *Palaeophyllophora* from *Hipposideros* (*Pseudorhinolophus*) and are likely to characterize both genera. These characters mainly concern the telencephalon area (Fig. 6a-d and 6h-k). *Hipposideros* (*Pseudorhinolophus*) has relatively smaller but also relatively higher and rounder olfactory bulbs, a wider angle of the orbitotemporal canal (Fig. 6h-k), a more marked sylvia but a less marked pseudosylvia, and more marked pyriform lobes; *Palaeophyllophora* species have more posteriorly located pyriform lobes. Regarding the diencephalon, the cast of the epiphysis (Fig. 6a-d) is also more marked in *Palaeophyllophora*. On the tectum of the mesencephalon, the shape and location of the rostral colliculi (Fig. 6a-d) make it possible to differentiate *Palaeophyllophora* species from *Hipposideros* fossil species described here: they are a little bit higher in *Hipposideros (Pseudorhinolophus)* and closer to each other and to the caudal colliculi (they are a bit more anterior in *Palaeophyllophora*, even closer to the epiphysis than to the caudal colliculi). The cerebellum (Fig. 6a-d) also allows one to distinguish the two genera: its anterior margin is more delineated in *Hipposideros* (*Pseudorhinolophus*), and the vermis and the cerebellar hemispheres are more aligned in this genus than in *Palaeophyllophora* (where the cerebellum is a bit more elongated and the cerebellar hemispheres are more anteriorly located relative to the vermis). Finally, cranial openings of the brain (Fig. 6e-g) also help to distinguish the two genera: (i) the optic foramina are much more anteriorly located in *H. (Ps.) bouziguensis* than in *Palaeophyllophora* species

(this is tempered by the quite bizarre position of these foramina in *H. (Ps.) bouziguensis*), (ii) the sphenorbital fissures are closer to each other and more anteriorly located in *Hipposideros* (*Pseudorhinolophus*), they are also a bit shorter and bear a small anterior notch (which is absent in *Palaeophyllophora*), and (iii) the foramen magnum opens more ventrally, whereas it opens more posteriorly in *Palaeophyllophora*. The telencephalic features observed in *H. (Ps.) bouziguensis* and *H. (Ps.) schlosseri* are also present in *H. diadema* (Fig. 9a and 9c). Other characteristics are difficult to compare finely between the brain of *H. diadema* and our endocast sample because the delineations of each part vary between an endocast and a brain, which is particularly true for exits of cranial nerves (see brain vs endocast comparisons above).

Potential trends within Hipposideridae

The three Paleogene species and the Miocene species differ by some characters that might show a temporal pattern. Among these is the posterior extension of the suprasylvia (Fig. 6a-d), which is absent in *Pa. quercyi* and in *H. (Ps.) schlosseri*, only starts to elongate posteriorly in *Pa. oltina*, and elongates a bit more in *H. (Ps.) bouziguensis* and in *H. diadema*. The two latter, Neogene, taxa also have more protruding caudal colliculi and a more convex (Fig. 6h-k) and more folded vermis (especially with a VI-VII sulcus present additionally to the other sulci already present; Fig. 6a-d and 6h-k).

H. (Ps.) schlosseri is the smallest species of the four. It differs from other species by characters of the cerebellum: the vermis is shallower (Fig. 6h-k), the cerebellar hemispheres are narrower and less protruding, and the intercrual sulci are less marked (Fig. 6a-d). These differences could be related to allometry.

Congruency between brain morphology, the temporal and the phylogenetic contexts

The phylogenetic context provided by Ravel et al. (2016) is rather robust: their matrix includes dental, cranial, and postcranial characters coded for a representative number of extinct hipposiderid taxa; their exact cladistic analysis retrieves a single parsimonious tree; and nodes have rather good support. However, of the four fossil species of our sample, two of them (*Pa. quercyi* and *H. (Ps.) schlosseri*) are only scored for dental characters and their phylogenetic position is therefore based on a single source of characters. On the other hand, the precise age of the specimens of these two species of our sample is unknown. Following Maitre (2014), *Pa. quercyi* is recorded from MP17a (early late Eocene, ~37 Mya) to MP22 (middle early Oligocene, ~31 Mya) and *H. (Ps.) schlosseri* is recorded from MP16 (late middle Eocene, ~38 Mya) to MP22. Given these uncertainties, other patterns of endocast morphological variation could be explained assuming different temporal and/or phylogenetic settings.

Regarding *H. (Ps.) schlosseri*, if swapping the relative positions of *H. (Ps.) schlosseri* and *H. (Ps.) bouziguensis* on the tree, all temporal characters distinguishing Paleogene vs Neogene fossil species would be regarded as phylogenetic characters (inducing a lot of changes at the *H. (Ps.) bouziguensis* – modern *Hipposideros* node).

In *Pa. quercyi*, several morphological characters distinguish this specimen from the others. For some characters, *Pa. quercyi* shows a morphological state and the three other species show another one: this pattern could be explained by a paraphyly of *Palaeophyllophora* with an early divergence of *Pa. quercyi*. These characters regard i) the olfactory bulbs (*Pa. quercyi* has the largest and longest of the sample; Table 1) and their lateral swelling (*Pa. quercyi* has the least developed of the sample; Fig. 6a-d); ii) the cerebrum, with a shallower anterior part of the rhinal fissure and a shallower sylvia (Fig.

6a-d and 6h-k), cerebral hemispheres much more separated, and less inflated lobes (reuniens, arcuate, and pyriform; Fig. 6h-k); and iii) the mesencephalon, which is the shallowest (tectum of mesencephalon is higher relative to cerebrum and cerebellum; Fig. 6h-k) and with caudal colliculi more rounded and farther from each other (Fig. 6a-d). For another character, *Pa. quercyi* shows a condition, while *Pa. oltina* and *H. (Ps.) schlosseri* show a second one, and *H. (Ps.) bouziguensis* shows a third one, reflecting a potential temporal pattern of morphological variation. This pattern is retrieved for the position of the orbitotemporal canal (more dorsally located in *Pa. quercyi*, a bit more lateral in *Pa. oltina* and *H. (Ps.) schlosseri*, and even more in *H. (Ps.) bouziguensis* and in *H. diadema*; Fig. 6a-d and 6h-k). The different hypotheses regarding these two morphological patterns are non-exclusive and could explain both patterns of morphological variation.

These various hypotheses are highly speculative but, given the uncertain temporal and phylogenetic context, such a set of morphological differences has to be taken into consideration and tentatively explained.

Conclusion

This work provides a revised nomenclature of the external structures of the Chiroptera brain and a detailed anatomical description of extinct hipposiderid bat endocranial casts. It constitutes the first thorough description of a chiropteran endocranial cast and sets the basis for future studies of this object at the ordinal scale. Generally, the new specimens described here greatly enhance our knowledge of brain macromorphology in fossil hipposiderid bats. Preliminary comparisons of extinct and extant hipposiderid bats brain external features indicate that, as previously proposed in the literature, endocranial casts are an accurate approximation of external features of the brain. Yet, some morphological traits such as cranial nerve pathways may not be fully reachable on endocranial cast. Based on our sample, the general morphology of the brain seems to be highly conservative within the hipposiderid family. Concurrently with this general morphological conservatism through Cenozoic times, there are no noticeable changes for usual measurements of endocasts (EQ, olfactory bulb volume, parafloccular volume). This apparent general homogeneity in hipposiderid brain characteristics is congruent with their general monotonous morphological diversity through time and may be linked to their conservative ecology. At a smaller scale, detailed comparisons further highlight several macromorphological features that could, for instance, separate *Palaeophyllophora* and *Hipposideros* genera. Fine anatomical characters, behind the global constant pattern and besides the reduced variation range induced by their ecological sophistication, could be of interest for tracking less apparent, maybe overlooked, but key morpho-anatomical evolution. These first results on fossil hipposiderid bat endocasts still rely on a small sample and a rather unclear phylogenetical context; future works at a wider scale and/or including extant species will allow for refining the different hypotheses proposed here.

Literature cited

Alba DM (2010) Cognitive inferences in fossil apes (Primates, Hominoidea): does encephalization reflect intelligence? J Anthropol Sci 88:11–48

Amador LI, Almeida FC, Giannini NP (2019) Evolution of traditional aerodynamic variables in bats (Mammalia: Chiroptera) within a comprehensive phylogenetic framework. J Mammal Evol. https://doi.org/10.1007/s10914-019-09475-8

Amador LI, Moyers Arévalo RL, Almeida FC, Catalano SA, Giannini NP (2018) Bat systematics in the light

of unconstrained analyses of a comprehensive molecular supermatrix. J Mammal Evol 25:37–70. https://doi.org/10.1007/s10914-016-9363-8

Anthony R, Grzybowski J de (1934) Le Neopallium du Boeuf. Etude de son Développement et Interprétation de ses Plissements. J Anat 68:558–70

Balanoff AM, Bever GS (2017) 1.10 The role of endocasts in the study of brain evolution. In: Kaas JH (ed) Evolution of Nervous Systems, 2nd edn. Academic Press, Oxford, pp 223–241

Baron G, Stephan H, Frahm HD (eds) (1996) Comparative Neurobiology in Chiroptera. Birkhäuser Verlag, Basel

Barone R, Bortolami R (eds) (2004) Anatomie comparée des mammifères domestiques : Tome 6, Neurologie I, Système nerveux central. Vigot, Paris

Benoit J (2015) A new method of estimating brain mass through cranial capacity in extinct proboscideans to account for the non-neural tissues surrounding their brain. J Vertebr Paleontol 35:e991021. https://doi.org/10.1080/02724634.2014.991021

Benoit J, Crumpton N, Mérigeaud S, Tabuce R (2013) A memory already like an elephant's? The advanced brain morphology of the last common ancestor of Afrotheria (Mammalia). Brain Behav Evol 81:154–169. https://doi.org/10.1159/000348481

Bertrand OC, Amador-Mughal F, Lang MM, Silcox MT (2018a) New virtual endocasts of Eocene Ischyromyidae and their relevance in evaluating neurological changes occurring through time in Rodentia. J Mammal Evol 26:345–371. https://doi.org/10.1007/s10914-017-9425-6

Bertrand OC, Amador-Mughal F, Lang MM, Silcox MT (2018b) Virtual endocasts of fossil Sciuroidea: brain size reduction in the evolution of fossoriality. Palaeontology 61:919–948. https://doi.org/10.1111/pala.12378

Bertrand OC, Shelley SL, Wible JR, Williamson TE, Holbrook LT, Chester SGB, Butler IB, Brusatte SL (2019) Virtual endocranial and inner ear endocasts of the Paleocene 'condylarth' *Chriacus* : new insight into the neurosensory system and evolution of early placental mammals. J Anat 236:21–49. https://doi.org/10.1111/joa.13084

Bertrand OC, Silcox MT (2016) First virtual endocasts of a fossil rodent: *Ischyromys typus* (Ischyromyidae, Oligocene) and brain evolution in rodents. J Vertebr Paleontol 36:. https://doi.org/10.1080/02724634.2016.1095762

Bhatnagar KP, Smith TD, Rai SN, Frahm HD (2016) The chiropteran brain database: volumetric survey of the hypophysis in 165 species. Anat Rec 299:492–510. https://doi.org/10.1002/ar.23321

Brown EE, Cashmore DD, Simmons NB, Butler RJ (2019) Quantifying the completeness of the bat fossil record. Palaeontology 62:757–776. https://doi.org/10.1111/pala.12426

Chambers JM, Hastie TJ (eds) (1991) Statistical Models in S. Chapman & Hall/CRC, London

Da Cruz A (2015) Photofiltre 7 [Computer Software]. Retrieved from http://www.photofiltre.com/

Dechaseaux C (1956) L'encéphale des mammifères volants. Colloq Int du Cent Natl la Rech Sci 80:51–58

Dechaseaux C (1962) Cerveaux d'animaux disparus. Masson et Cie, Paris

Dechaseaux C (1970) Récents résultats en paléoneurologie. Bull Académie Société Lorraines des Sci 9:223–232

Dechaseaux C (1973) Essais de paléoneurologie. Ann Paléontol 59:8–132

Dow RS (1942) The evolution and anatomy of the cerebellum. Biol Rev 17:179–220. https://doi.org/10.1111/j.1469-185X.1942.tb00437.x

Dunn OJ (1964) Multiple comparisons using rank sums. Technometrics 6:241. https://doi.org/10.2307/1266041

Edinger T (1926) Fossile Fledermausgehirne. Senckenbergiana 8:1–16

Edinger T (1929) Die fossilen Gehirne. Ergeb Anat Entwicklungsgesch 28:1–249

Edinger T (1949) Paleoneurology vs comparative brain anatomy. Confin Neurol 9:5–24

Edinger T (1961) Fossil brains reflect specialized behavior. World Neurol 2:934–41

Edinger T (1963) Meanings of midbrain exposure, past and present. In: XVI International Congress of Zoology. pp 225–228

Edinger T (1964a) Midbrain exposure and overlap in mammals. Am Zool 4:5–19. https://doi.org/10.2307/3881308

Edinger T (1964b) Recent advances in paleoneurology. Prog Brain Res 6:147–160. https://doi.org/10.1016/S0079-6123(08)63721-8

Eisenberg JF, Wilson DE (1978) Relative brain size and feeding strategies in the Chiroptera. Evolution 32:740. https://doi.org/10.2307/2407489

Eiting TP, Gunnell GF (2009) Global completeness of the bat fossil record. J Mammal Evol 16:151–173. https://doi.org/10.1007/s10914-009-9118-x

Felsenstein J (1985) Phylogenies and the comparative method. Am Nat 125:1–15

Ferreira-Cardoso S, Araújo R, Martins NE, Martins GG, Walsh S, Martins RMS, Kardjilov N, Manke I, Hilger A, Castanhinha R (2017) Floccular fossa size is not a reliable proxy of ecology and behaviour in vertebrates. Sci Rep 7:2005. https://doi.org/10.1038/s41598-017-01981-0

Fisher SRA (1970) Statistical Methods for Research Workers, 14th edn. Oliver and Boyd, Edinburgh

Foley NM, Goodman SM, Whelan CV, Puechmaille SJ, Teeling EC (2017) Towards navigating the Minotaur's labyrinth: cryptic diversity and taxonomic revision within the speciose genus *Hipposideros* (Hipposideridae). Acta Chiropterol 19:1–18. https://doi.org/10.3161/15081109ACC2017.19.1.001

Foley NM, Thong VD, Soisook P, Goodman SM, Armstrong KN, Jacobs DS, Puechmaille SJ, Teeling EC (2015) How and why overcome the impediments to resolution: lessons from rhinolophid and hipposiderid bats. Mol Biol Evol 32:313–333. https://doi.org/10.1093/molbev/msu329

Friant M (1932) L'influence de la taille sur la morphologie des dents chez les mammifères. La Terre la

Vie 135–144

Friant M (1954) Le cerveau du Lamantin (*Manatus inunguis* Natterer). Vierteljahrsschrift der Naturforschenden Gesellschaft Zürich 99:129–135

Giannini NP, Wible JR, Simmons NB (2006) On the cranial osteology of Chiroptera. I. *Pteropus* (Megachiroptera: Pteropodidae). Bull Am Mus Nat Hist 295:1–134. https://doi.org/10.1206/0003-0090(2006)295[0001:OTCOOC]2.0.CO;2

Gingerich PD (2016) Body weight and relative brain size (encephalization) in Eocene Archaeoceti (Cetacea). J Mammal Evol 23:17–31. https://doi.org/10.1007/s10914-015-9304-y

Gonzales LA, Benefit BR, McCrossin ML, Spoor F (2015) Cerebral complexity preceded enlarged brain size and reduced olfactory bulbs in Old World monkeys. Nat Commun 6:7580. https://doi.org/10.1038/ncomms8580

Grafen A (1989) The phylogenetic regression. Philos Trans R Soc B Biol Sci 326:119–157. https://doi.org/10.1098/rstb.1989.0106

Hand SJ, Kirsch JAW (2003) *Archerops*, a new annectent hipposiderid genus (Mammalia : Microchiroptera) from the Australian Miocene. J Paleontol 77:1139–1151. https://doi.org/10.1666/0022-3360(2003)077<1139:AANAHG>2.0.CO;2

Hollander M, Wolfe DA (1973) Nonparametric Statistical Methods. John Wiley & Sons, New York

Horikawa J, Suga N (1986) Biosonar signals and cerebellar auditory neurons of the mustached bat. J Neurophysiol 55:1247–1267. https://doi.org/10.1152/jn.1986.55.6.1247

Inkscape Project (2018) Inkscape [Computer software]. Retrieved from https://inkscape.org/

Ito M (1982) Cerebellar control of the vestibulo-ocular reflex--around the flocculus hypothesis. Annu Rev Neurosci 5:275–297. https://doi.org/10.1146/annurev.ne.05.030182.001423

Jerison HJ (1973) Evolution of the Brain and Intelligence. Academic Press, New York

Jolicoeur P, Pirlot P, Baron G, Stephan H (1984) Brain structure and correlation patterns in Insectivora, Chiroptera, and Primates. Syst Biol 33:14–29. https://doi.org/10.1093/sysbio/33.1.14

Jones KE, Bininda-Emonds ORP, Gittleman JL (2005) Bats, clocks, and rocks: diversification patterns in Chiroptera. Evolution 59:2243–2255. https://doi.org/10.1554/04-635.1

Kelava I, Lewitus E, Huttner WB (2013) The secondary loss of gyrencephaly as an example of evolutionary phenotypical reversal. Front Neuroanat 7:1–9. https://doi.org/10.3389/fnana.2013.00016

Kochetkova VI (1978) The subject matter of paleoneurological studies. In: Kochetkova VI, Jerison HJ, Jerison I (eds) Paleoneurology. V. H. Winston & Sons, Washington, D.C., pp 17–45

Kruskal WH, Wallis WA (1952) Use of ranks in one-criterion variance analysis. J Am Stat Assoc 47:583–621. https://doi.org/10.1080/01621459.1952.10483441

Larsell O, Dow RS (1935) The development of the cerebellum in the bat (*Corynorhinus* sp.) and certain other mammals. J Comp Neurol 62:443–468. https://doi.org/10.1002/cne.900620210

Lebrun R (2018) MorphoDig, an open-source 3D freeware dedicated to biology

Legendre S (1982) Hipposideridae (Mammalia: Chiroptera) from the Mediterranean middle and late Neogene, and evolution of the genera *Hipposideros* and *Asellia*. J Vertebr Paleontol 2:372–385. https://doi.org/10.1080/02724634.1982.10011939

Maitre E (2014) Western European middle Eocene to early Oligocene Chiroptera: systematics, phylogeny and palaeoecology based on new material from the Quercy (France). Swiss J Palaeontol 133:141–242. https://doi.org/10.1007/s13358-014-0069-3

Mein P (1975) Résultats du groupe de travail des vertébrés: biozonation du Neogène méditerranéen à partir des mammifères. In: Senes J (ed) Report on Activity of the RCMNS (Regional Committee on Mediterranean Neogene Stratigraphy) Working Groups (1971–1975). Bratislava, pp 78–81

Millien V, Bovy H (2010) When teeth and bones disagree: body mass estimation of a giant extinct rodent. J Mammal 91:11–18. https://doi.org/10.1644/08-MAMM-A-347R1.1.Key

Muizon C de, Billet G, Argot C, Ladevèze S, Goussard F (2015) *Alcidedorbignya inopinata*, a basal pantodont (Placentalia, Mammalia) from the early Palaeocene of Bolivia: anatomy, phylogeny and palaeobiology. Geodiversitas 37:397–631. https://doi.org/10.5252/g2015n4a1

Neubauer S (2014) Endocasts: possibilities and limitations for the interpretation of human brain evolution. Brain Behav Evol 84:117–134. https://doi.org/10.1159/000365276

Nieuwenhuys R (1998) Morphogenesis and general structure. In: Nieuwenhuys R, ten Donkelaar HJ, Nicholson C (eds) The Central Nervous System of Vertebrates. Springer Berlin Heidelberg, Berlin, Heidelberg, pp 159–228

Nomina Anatomica Veterinaria (NAV) (2017) International Committee on Veterinary Gross Anatomical Nomenclature (I.C.V.G.A.N.), 6th edn. The Editorial Committee with permission of the World Association of Veterinary Anatomists (W.A.V.A.), Hanover (Germany), Ghent (Belgium), Columbia, MO (USA), Rio de Janeiro (Brazil)

Ogle DH, Wheeler P, Dinno A (2019) FSA: Fisheries Stock Analysis. R package version 0.8.30.9000, https://github.com/droglenc/FSA

Orliac MJ, Gilissen E (2012) Virtual endocranial cast of earliest Eocene *Diacodexis* (Artiodactyla, Mammalia) and morphological diversity of early artiodactyl brains. Proc R Soc B Biol Sci 279:3670–3677. https://doi.org/10.1098/rspb.2012.1156

Orliac MJ, O'Leary MA (2014) Comparative anatomy of the petrosal bone of dichobunoids, early members of Artiodactylamorpha (Mammalia). J Mammal Evol 21:299–320. https://doi.org/10.1007/s10914-014-9254-9

Orlov YA (ed) (1961) В мире древних животных (In the ancient animal kingdom). Publishing House of the Academy of Sciences of the USSR, Moscow

Paulin MG (1993) The role of the cerebellum in motor control and perception. Brain Behav Evol 41:39–50. https://doi.org/10.1159/000113822

R Core Team (2018) R: A Language and Environment for Statistical Computing. R Foundation for Statistical Computing, Vienna, Austria. https://www.r-project.org/

Rambold H, Churchland A, Selig Y, Jasmin L, Lisberger SG (2002) Partial ablations of the flocculus and ventral paraflocculus in monkeys cause linked deficits in smooth pursuit eye movements and adaptive modification of the VOR. J Neurophysiol 87:912–924. https://doi.org/10.1152/jn.00768.2000

Ramdarshan A, Orliac MJ (2016) Endocranial morphology of *Microchoerus erinaceus* (Euprimates, Tarsiiformes) and early evolution of the Euprimates brain. Am J Phys Anthropol 159:5–16. https://doi.org/10.1002/ajpa.22868

Ravel A, Adaci M, Bensalah M, Charruault AL, Essid EM, Ammar HK, Marzougui W, Mahboubi M, Mebrouk F, Merzeraud G, Vianey-Liaud M, Tabuce R, Marivaux L (2016) Origine et radiation initiale des chauves-souris modernes : nouvelles découvertes dans l'Éocène d'Afrique du Nord. Geodiversitas 38:355–434. https://doi.org/10.5252/g2016n3a3

Rowe TB, Macrini TE, Luo Z-X (2011) Fossil evidence on origin of the mammalian brain. Science 332:955–957. https://doi.org/10.1126/science.1203117

Royston P (1995) Remark AS R94: a remark on algorithm AS 181: the W-test for normality. Appl Stat 44:547. https://doi.org/10.2307/2986146

RStudio Team (2016) RStudio: Integrated Development Environment for R. RStudio, PBC, Boston, MA. http://www.rstudio.com/

Safi K, Seid MA, Dechmann DKN (2005) Bigger is not always better: when brains get smaller. Biol Lett 1:283–286. https://doi.org/10.1098/rsbl.2005.0333

Schmidt-Kittler N (ed) (1987) International Symposium on Mammalian Biostratigraphy and Palaeoecology of the European Paleogene-Mainz, February 18th–21st 1987. Münchner Geowissenschaftliche Abhandlungen A 10:1–312

Schneider CA, Rasband WS, Eliceiri KW (2012) NIH Image to ImageJ: 25 years of image analysis. Nat Methods 9:671–675. https://doi.org/10.1038/nmeth.2089

Shapiro SS, Wilk MB (1965) An analysis of variance test for normality (complete samples). Biometrika 52:591–611. https://doi.org/10.1093/biomet/52.3-4.591

Shi JJ, Rabosky DL (2015) Speciation dynamics during the global radiation of extant bats. Evolution (N Y) 69:1528–1545. https://doi.org/10.1111/evo.12681

Shultz S, Dunbar R (2010) Encephalization is not a universal macroevolutionary phenomenon in mammals but is associated with sociality. Proc Natl Acad Sci USA 107:21582–21586. https://doi.org/10.1073/pnas.1005246107

Sigé B (1968) Les Chiroptères du Miocène inférieur de Bouzigues. 1- Etude systématique. Palaeovertebrata 1:65–133. https://doi.org/10.18563/pv.1.3.65-133

Sigé B, Crochet J-Y, Sudre J, Aguilar JP, Escarguel G (1997) Nouveaux sites d'âges variés dans les remplissages karstiques du Miocène inférieur de Bouzigues (Hérault, Sud de la France). Geobios 30:477–483. https://doi.org/10.1016/S0016-6995(97)80054-X

Silcox MT, Benham AE, Bloch JI (2010) Endocasts of *Microsyops* (Microsyopidae, Primates) and the evolution of the brain in primitive primates. J Hum Evol 58:505–521.

https://doi.org/10.1016/j.jhevol.2010.03.008

Silcox MT, Dalmyn CK, Bloch JI (2009) Virtual endocast of *Ignacius graybullianus* (Paromomyidae, Primates) and brain evolution in early primates. Proc Natl Acad Sci USA 106:10987–10992. https://doi.org/10.1073/pnas.0812140106

Simmons NB (2000) Bat phylogeny: an evolutionary context for comparative studies. In: Adams RA, Pedersen SC (eds) Ontogeny, Functional Ecology, and Evolution of Bats. Cambridge University Press, New-York, pp 9–58

Simmons NB (2005) Chiroptera. In: Rose KD, Archibald JD (eds) The Rise of Placental Mammals. John Hopkins University Press, Baltimore, pp 159–174

Simmons NB, Geisler JH (1998) Phylogenetic relationships of *Icaronycteris*, *Archaeonycteris*, *Hassianycteris*, and *Palaeochiropteryx* to extant bat lineages, with comments on the evolution of echolocation and foraging strategies in Microchiroptera. Bull Am Mus Nat Hist 235:1–182

Simmons NB, Seymour KL, Habersetzer J, Gunnell GF (2008) Primitive early Eocene bat from Wyoming and the evolution of flight and echolocation. Nature 451:818–821. https://doi.org/10.1038/nature06549

Smith GE (1902a) On the homologies of the cerebral sulci. J Anat Physiol 36:309–319

Smith GE (1902b) The primary subdivision of the mammalian cerebellum. J Anat Physiol 36:381–5

Smith RJ (2002) Estimation of body mass in paleontology. J Hum Evol 43:271–287. https://doi.org/10.1006/jhev.2002.0573

Takai M, Shigehara N, Egi N, Tsubamoto T (2003) Endocranial cast and morphology of the olfactory bulb of *Amphipithecus mogaungensis* (latest middle Eocene of Myanmar). Primates 44:137–144. https://doi.org/10.1007/s10329-002-0027-3

Teeling EC (2009) Bats (Chiroptera). In: Hedges SB, Kumar S (eds) The Timetree of Life. Oxford University Press, New York, pp 499–503

Teeling EC, Madsen O, Van Den Bussche RA, De Jong WW, Stanhope MJ, Springer MS (2002) Microbat paraphyly and the convergent evolution of a key innovation in old world rhinolophoid microbats. Proc Natl Acad Sci U S A 99:1431–1436. https://doi.org/10.1073/pnas.022477199

Teeling EC, Scally M, Kao DJ, Romagnoli ML, Springer MS, Stanhope MJ (2000) Molecular evidence regarding the origin of echolocation and flight in bats. Nature 403:188–192. https://doi.org/10.1038/35003188

Tukey JW (1949) Comparing Individual Means in the Analysis of Variance. Biometrics 5:99. https://doi.org/10.2307/3001913

van Dongen PAM (1998) Brain size in vertebrates. In: Nieuwenhuys R, ten Donkelaar HJ, Nicholson C (eds) The Central Nervous System of Vertebrates. Springer Berlin Heidelberg, Berlin, Heidelberg, pp 2099–2134

Voogd J, Nieuwenhuys R, van Dongen PAM, ten Donkelaar HJ (1998) Mammals. In: Nieuwenhuys R, ten Donkelaar HJ, Nicholson C (eds) The Central Nervous System of Vertebrates. Springer Berlin

Heidelberg, Berlin, Heidelberg, pp 1637–2097

Voogd J, Wylie DRW (2004) Functional and anatomical organization of floccular zones: a preserved feature in vertebrates. J Comp Neurol 470:107–112. https://doi.org/10.1002/cne.11022

Waespe W, Cohen B, Raphan T (1983) Role of the flocculus and paraflocculus in optokinetic nystagmus and visual-vestibular interactions: effects of lesions. Exp Brain Res 50:. https://doi.org/10.1007/BF00238229

Wilson LAB, Hand SJ, López-Aguirre C, Archer M, Black KH, Beck RMD, Armstrong KN, Wroe S (2016) Cranial shape variation and phylogenetic relationships of extinct and extant Old World leaf-nosed bats. Alcheringa An Australas J Palaeontol 40:509–524. https://doi.org/10.1080/03115518.2016.1196434

Yao L, Brown J-P, Stampanoni M, Marone F, Isler K, Martin RD (2012) Evolutionary change in the brain size of bats. Brain Behav Evol 80:15–25. https://doi.org/10.1159/000338324

Figures

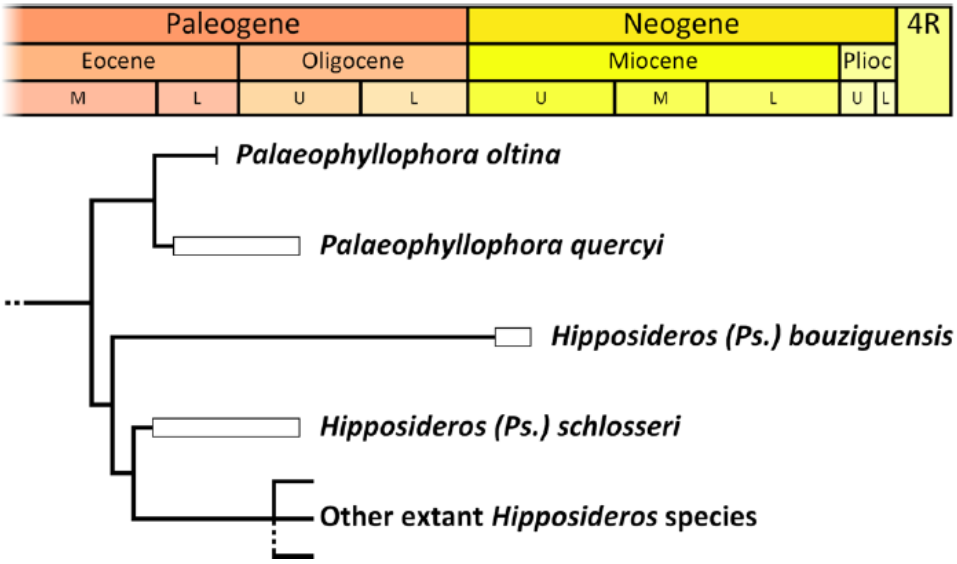

Fig. 1 Phylogenetic relationships and temporal occurrences over the last 45 Million years of the four fossil species studied here. Ages of *Pa. quercyi*, *Pa. oltina*, and *H. (Ps.) schlosseri* after Maitre (2014). Ages of *H. (Ps.) bouziguensis* after Sigé (1968). Age of "extant *Hipposideros* species" node after Foley et al. (2015, 2017)

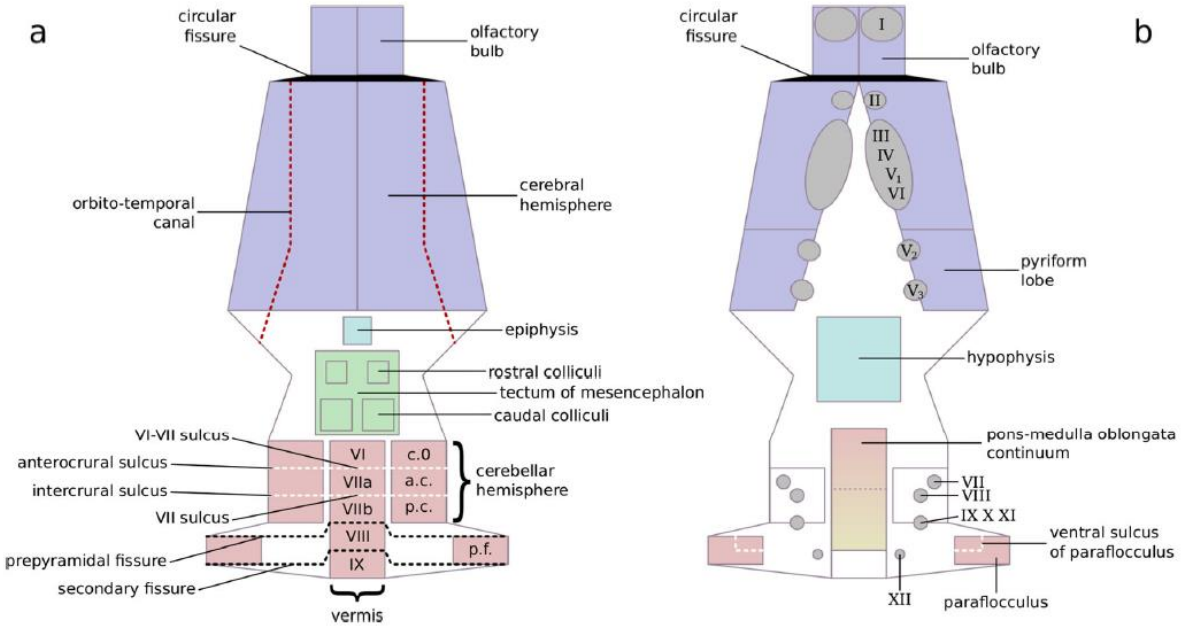

Fig. 2 Illustration of the nomenclature of a theoretical chiropteran endocast in dorsal (a) and ventral (b) views. The main subdivisions of the brain are in blue (telencephalon), light blue (diencephalon), green (mesencephalon), red (metencephalon) and yellow (myelencephalon). The color gradient from red to yellow of the pons-medulla oblongata continuum and the dashed mid-line indicate that both structures cannot be macromorphologically distinguished. Roman numbers indicate the corresponding cranial nerve exits. Abbreviations are: c.0-crus 0 of the cerebellar hemisphere; a.c.-anterior crus of the cerebellar hemisphere; p.c.-posterior crus of the cerebellar hemisphere; p.f.-paraflocculus.

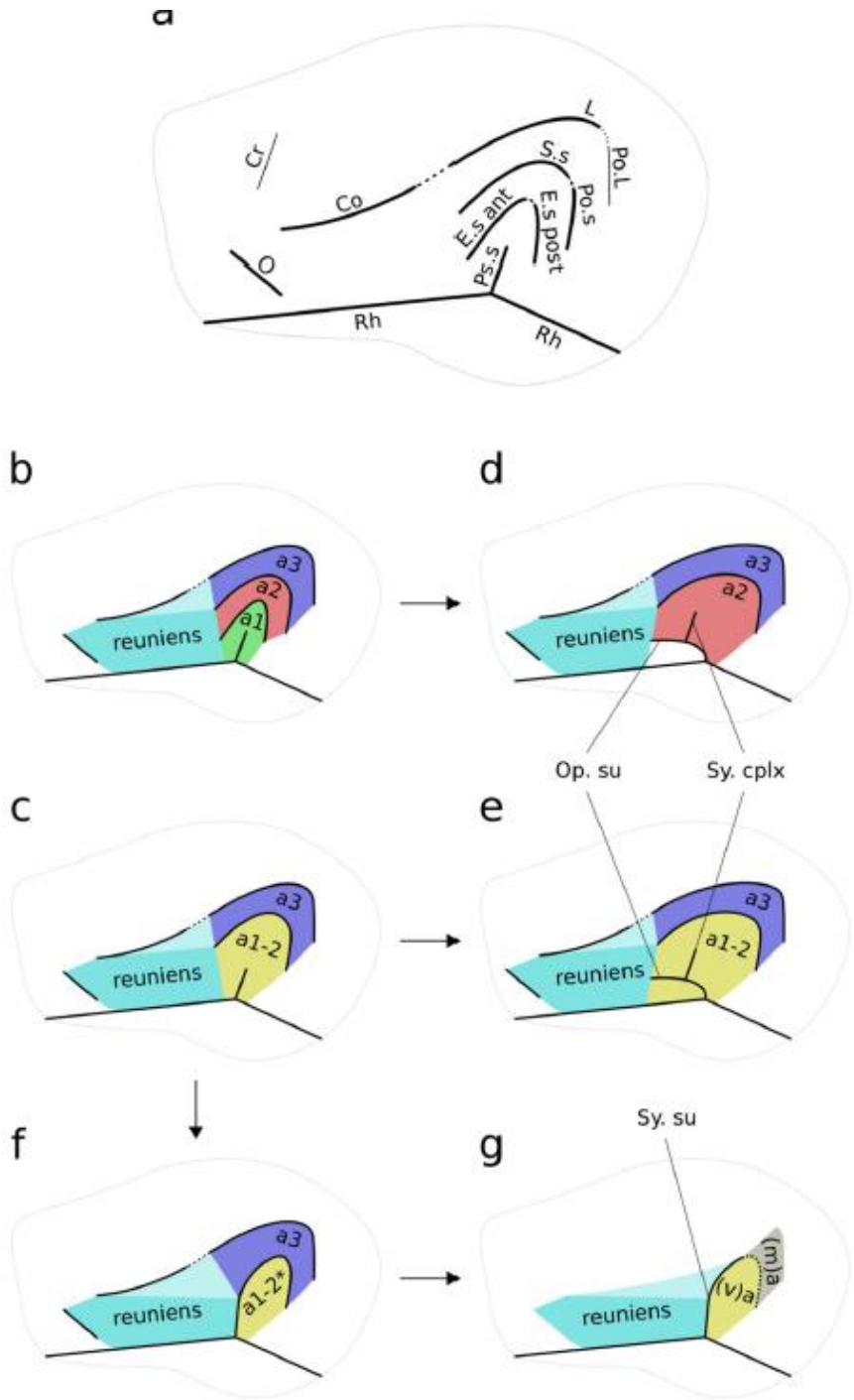

Fig. 3 Illustration of the nomenclature of primary sulci (**a**) and areas (**b-c**) of a theoretical brain and of primary changes of brain morphology (**d-g**) mainly following the hypotheses of Dechaseaux (1962). Arrows from b to d and from c to e show the operculization of the arcuate gyrus 1 by the arcuate gyrus 2 (b to d) or of the arcuate gyrus 2 by itself (c to e). The arrow from c to f indicates the formation of the sylvia by merging the posterior end of the pseudosylvia and the anterior end of the suprasylvia. The arrow from f to g indicates the transition from a "sylvian sulcus" theoretical condition to a "hipposiderid bat" theoretical condition, with the absence of orbital, coronal and lateral sulci and by the disparate presence or absence of the posterior extension of the suprasylvia, which therefore separates (or not when absent) the arcuate lobe ("a") in the ventral and medial arcuate lobes ("(v) a" and "(m) a"). Sulci abbreviations: **Co**-coronal (sulcus), **Cr**-cruciate (sulcus), **E.s ant**-anterior part of ectosylvia(n sulcus), **E.s post**-posterior part of ectosylvia(n sulcus), **L**-lateral (sulcus), **O**-orbital (sulcus),

Op. su-operculization sulcus, **Po.L**-postlateral (sulcus), **Po.s**-postsylvia(n sulcus), **Ps.s**-pseudosylvia(n sulcus), **Rh**-rhinal fissure, **S.s**-suprasylvia(n sulcus), **Sy. Cplx**-sylvian complex, **Sy. Su**-sylvia(n sulcus). Areas abbreviations: **a1**-arcuate gyrus 1, **a2**-arcuate gyrus 2, **a3**-arcuate gyrus 3, **a1-2**-arcuate gyrus 1-2, **a1-2***-posterior arm of arcuate gyrus 1-2, **(v)a** and **(d)a**-(ventral) and (dorsal) arcuate lobe respectively

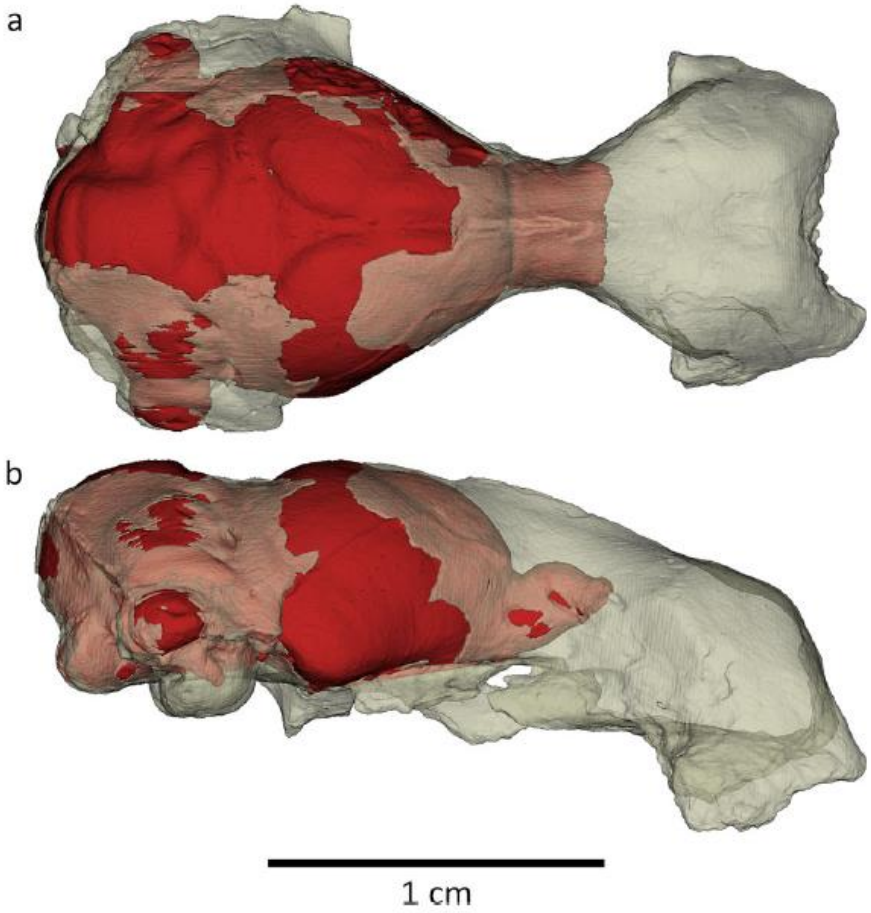

Fig. 4 Skull (transparent) and endocranial cast (red) of *Palaeophyllophora oltina* (NMBS QP784) in dorsal (a) and lateral right (b) views

Fig. 4 Skull (transparent) and endocranial cast (red) of *Palaeophyllophora oltina* (NMBS QP 784) in dorsal (**a**) and lateral right (**b**) views

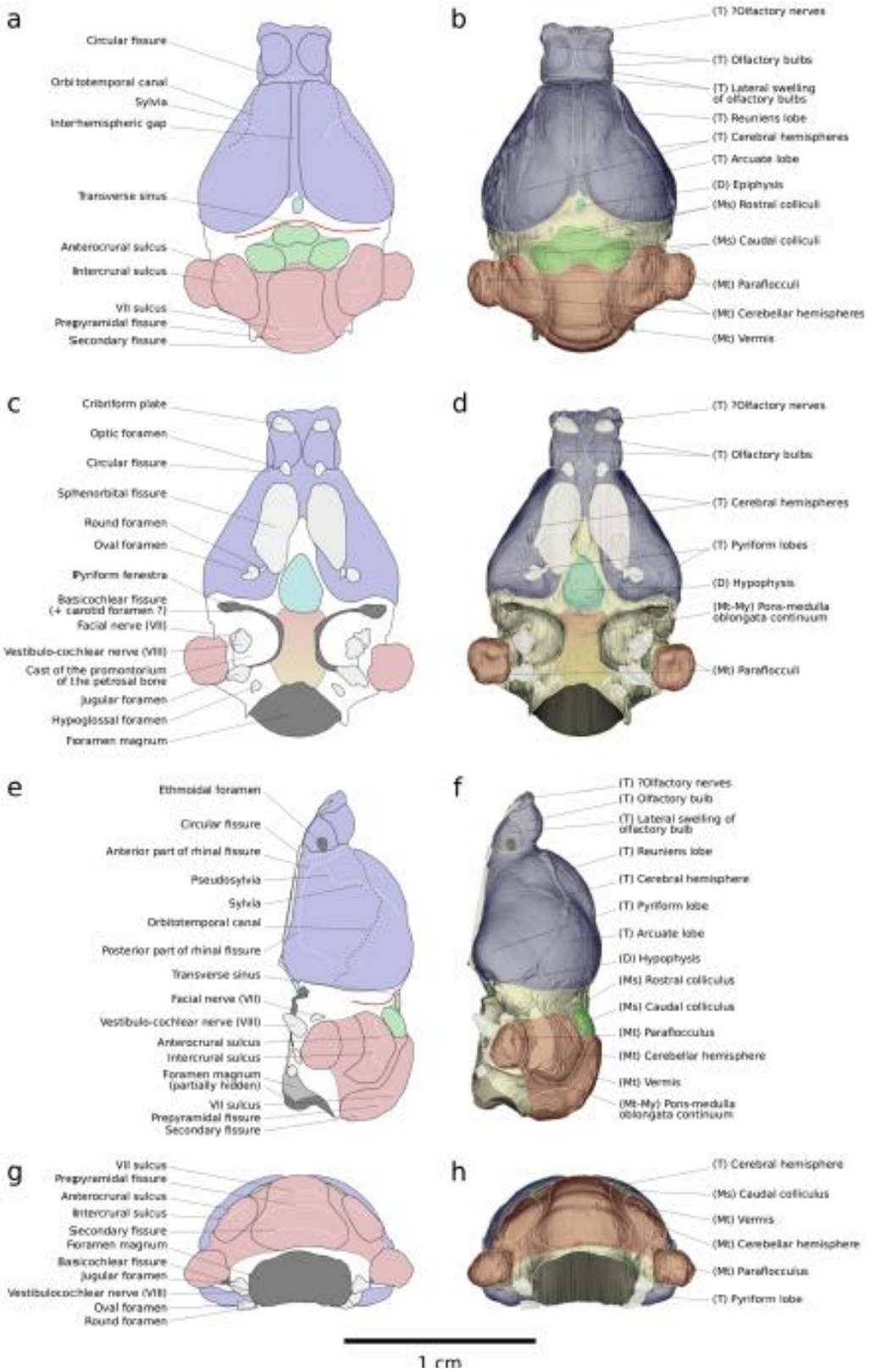

Fig. 5 Endocranial cast of *Palaeophyllophora oltina* (NMBS QP 784) in dorsal (**a-b**), ventral (**c-d**), lateral right mirrored (**e-f**) and occipital (**g-h**) views. Right figures (b,d,f,h) illustrates the endocranial cast with the main subdvisions of the brain (blue/T-telencephalon, light blue/D-diencephalon, green/Ms-mesencephalon, yellow/Mt-metencephalon, red/My-myelencephalon). Left figures (a,c,e,g) illustrates the different casts (blood vessels, red) and grooves (sulci and fissures, white) of these areas, and the casts of cranial nerve exits (light white) and other cranial foramina (dark grey)

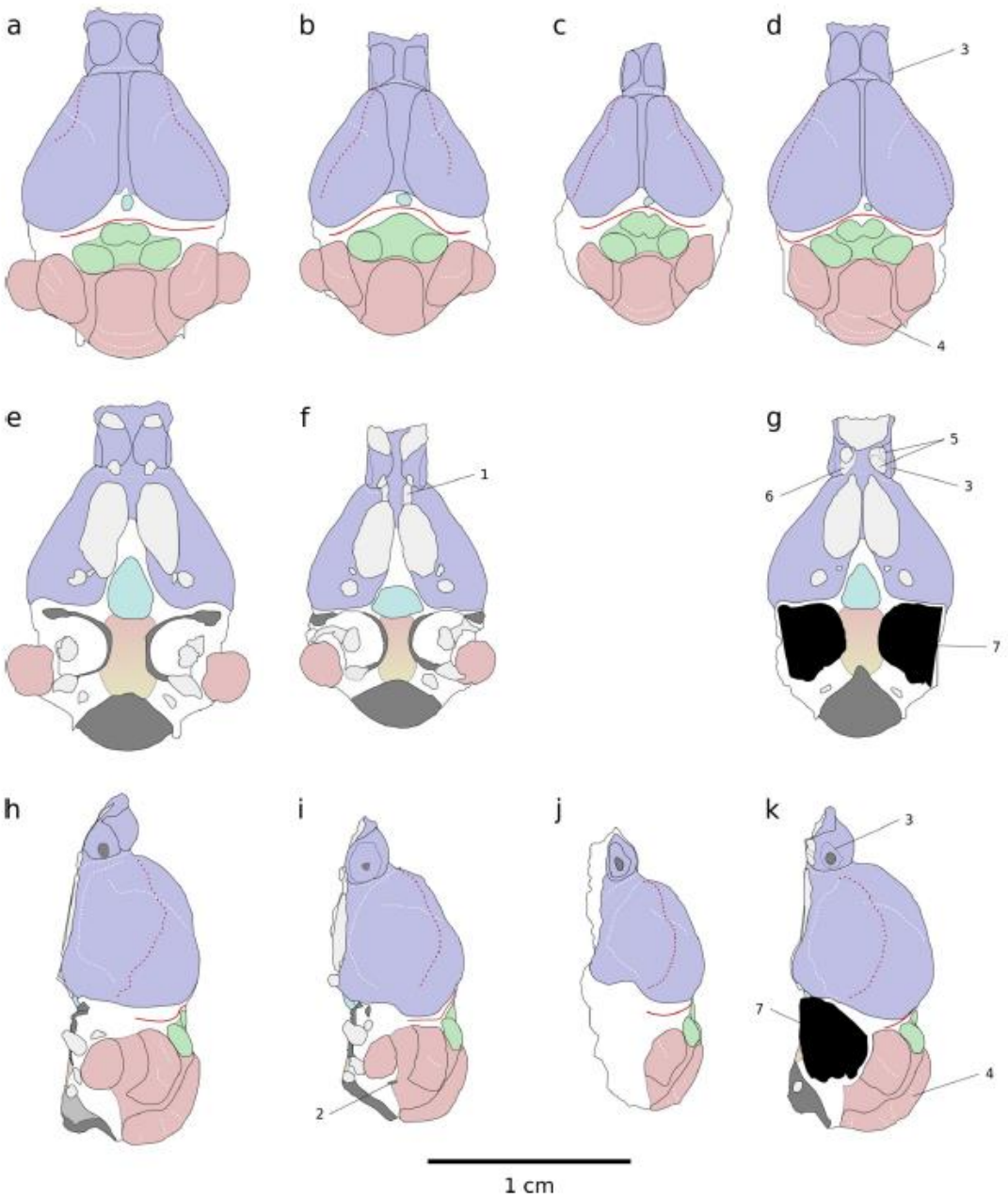

Fig. 6 Comparative schemes (as for Fig. 5a,c,e,g) of the fossil sample endocasts studied here in dorsal (**a-d**), ventral (**e-g**) and lateral (**h-k**) views. From left to right: *Palaeophyllophora oltina* (NMBS QP 784; a,e,h), *Palaeophyllophora quercyi* (UM ACQ 6627; b,f,i), *Hipposideros (Pseudorhinolophus) schlosseri* (NMBS QV 370; c,j) and *Hipposideros (Pseudorhinolophus) bouziguensis* (NMBS Q2369; d,g,k). Numbers highlight absent structures in *Pa. oltina*: **1**-optic canal, **2**-mastoid foramen, **3**-shallow delineation of the lateral swelling of the olfactory bulb, **4**-VI-VII sulcus of the vermis, **5**-two "sub-foramina" of what is considered as the single left optic foramen in *H. (Ps.) bouziguensis*, **6**-potential posterior extent of the right optic foramen in *H. (Ps.) bouziguensis*, **7**-absence of petrosals

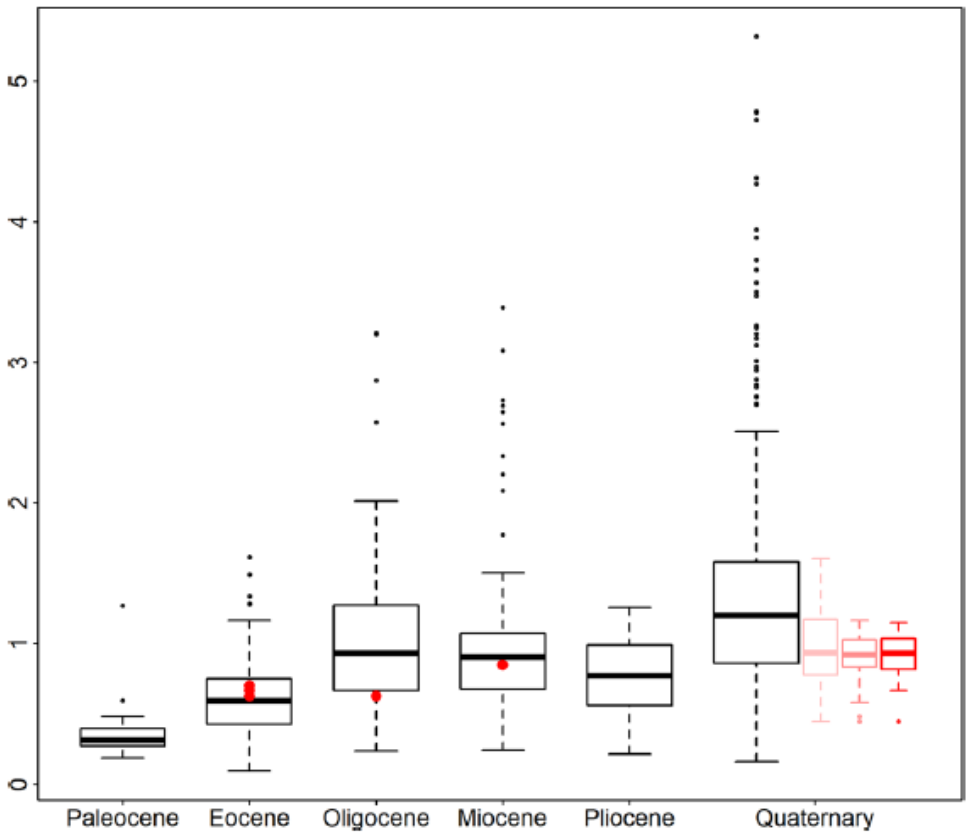

Fig. 7 Boxplot of EQ values (y-axis) following Eisenberg & Wilson's formula (Eisenberg and Wilson 1978) in mammals through cenozoic epochs (x-axis). Black boxplots: all mammals except bats. Light pink boxplot: bats. Pink boxplot: extant rhinolophoids. Red boxplot: extant hipposiderids. Red dots: extinct hipposiderids (with *H. (Ps.) schlosseri* represented in Eocene and in Oligocene)

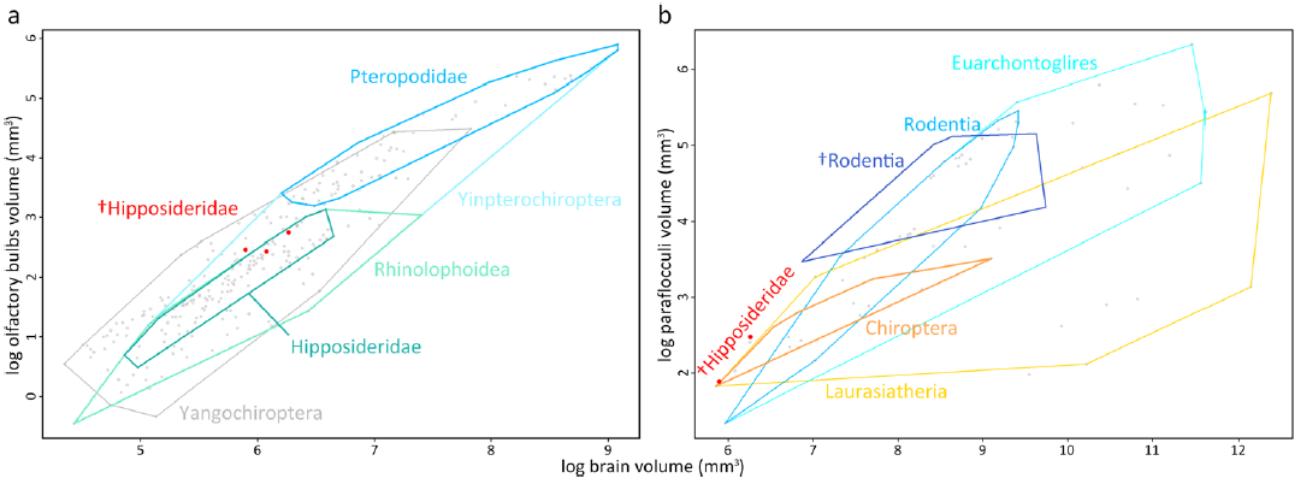

Fig. 8 Biplots of olfactory bulbs log-volume (**a**; y-axis) and paraflocculi log-volume (**b**; y-axis) relative to whole brain log-volume (x-axis). Biplot of olfactory bulb vs whole brain log-volumes (a) is at the Chiroptera scale, with the morphospaces of the two sub-orders (Yangochiroptera, Yinpterochiroptera), the two sub-clades of Yinpterochiroptera (Pteropodidae, Rhinolophoidea) and the extant family of the fossil sample in Rhinolophoidea (Hipposideridae). Biplot of paraflocculi vs whole brain log-volumes (b) is at the Mammalia scale, with the morphospaces of the super-order (Euarchontoglires and Laurasiatheria) and of the order (Rodentia and Chiroptera) of the other extinct mammals for which

data is available (ischyromyid rodents, with enough points to draw another morphospace, and hipposiderid bats, with only two points).

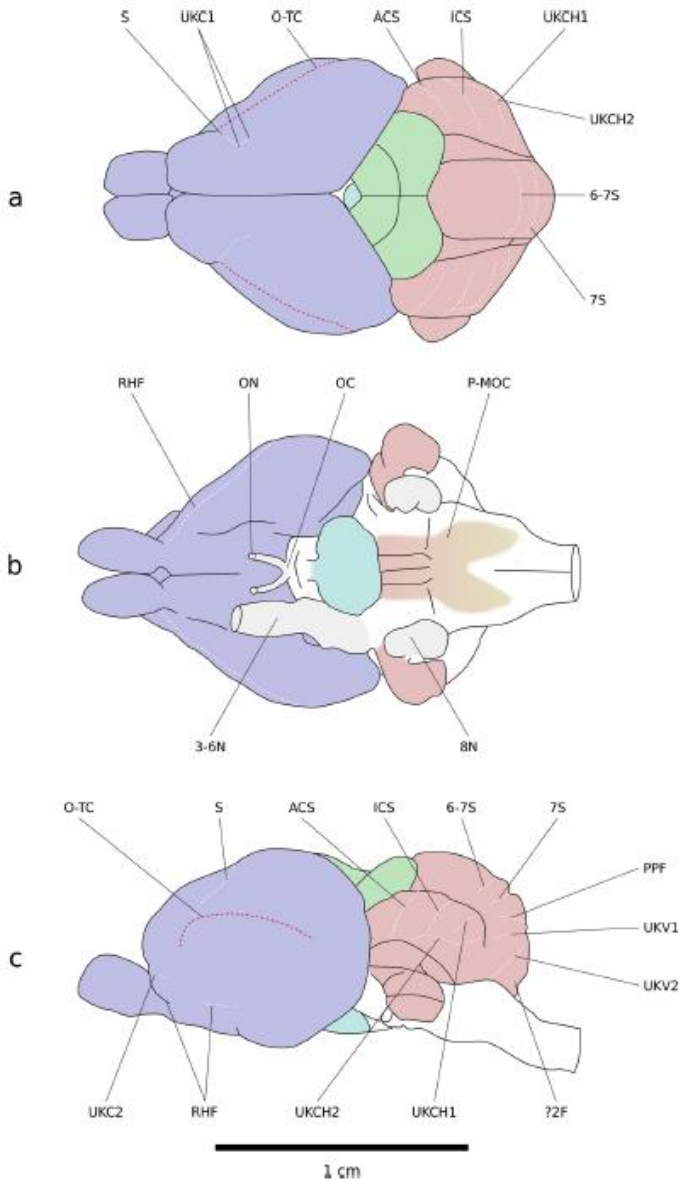

Fig. 9 Interpretation (following that of Figs. 5a,c,e,g and 6) of the illustration of the brain of *Hipposideros diadema* by Baron et al. (1996) in dorsal (**a**; Baron et al. 1996: fig. 8), ventral (**b**; Baron et al. 1996: fig. 40) and lateral (**c**; Baron et al. 1996: fig. 24) views. Except for the pons-medulla oblongata continuum (**P-MOC**), other captions indicates pathways: **?2F**-?secondary fissure, **3-6N**-bundle of cranial nerves III to VI, **6-7S**-VI-VII sulcus, **7S**-VII sulcus, **8N**-vestibulocochlear cranial nerve VIII, **ACS**-anterocrural sulcus, **ICS**-intercrural sulcus, **OC**-optic chiasm, **ON**-optic nerve, **O-TC**-orbitotemporal canal, **PPF**-prepyramidal fissure, **RHF**-rhinal fissure, **S**-sylvia, **UKC1**- and **UKC2**-unknown sulci of the cerebral hemispheres 1 and 2, **UKCH1**- and **UKCH2**-unknown sulci of the cerebellar hemispheres 1 and 2, **UKV1**- and **UKV2**-unknown sulci of the vermis 1 and 2.